The Cryosphere Discuss., doi:10.5194/tc-2017-17, 2017
Manuscript under review for journal The Cryosphere
Discussion started: 21 February 2017

The Cryosphere Discussions
Open Access
EGU

Distinguishing between old and modern permafrost sources with compound-specific δ^2H analysis

Jorien E. Vonk[1], Tommaso Tesi[2,3], Lisa Bröder[2,4], Henry Holmstrand[2,4], Gustaf Hugelius[4,5], August Andersson[2,4], Oleg Dudarev[6,7], Igor Semiletov[6,7,8], Örjan Gustafsson[2,4]

[1] Department of Earth Sciences, VU University, The Netherlands
[2] Department of Environmental Science and Analytical Chemistry, Stockholm University, Sweden
[3] ISMAR Institute of Marine Sciences, Bologna, Italy
[4] Bolin Centre for Climate Research, Stockholm University, Sweden
[5] Department of Physical Geography, Stockholm University, Sweden
[6] Pacific Oceanological Institute FEBRAS, Vladivostok, Russia
[7] Tomsk Polytechnic University, Tomsk, Russia
[8] University of Alaska Fairbanks, Fairbanks, USA

Correspondence to: Jorien Vonk (j.e.vonk@vu.nl)

Keywords: deuterium isotopes, yedoma, ice complex deposit, n-alkanoic acids, n-alkanes, organic matter, stable carbon isotopes, radiocarbon, Siberian Arctic, sediments, permafrost thaw

Abstract

Pleistocene ice complex permafrost deposits contain roughly a quarter of the organic carbon (OC) stored in permafrost terrain. When permafrost thaws, its OC is remobilized into the (aquatic) environment where it is available for degradation, transport or burial. Aquatic or coastal environments contain sedimentary reservoirs that can serve as archives of past climatic change. As permafrost thaw is increasing throughout the Arctic, these reservoirs are important locations to assess the fate of remobilized permafrost OC.

We here present compound-specific deuterium (δ^2H) analysis on leaf waxes as a tool to distinguish between OC released from thawing Pleistocene permafrost (Ice Complex Deposits; ICD) and from thawing Holocene permafrost (from near-surface soils). Bulk geochemistry (%OC, $\delta^{13}C$, %total nitrogen; TN) was analyzed as well as the concentrations and δ^2H signatures of long-chain *n*-alkanes (C_{21} to C_{33}) and mid/long-chain *n*-alkanoic acids (C_{16} to C_{30}) extracted from both ICD-PF samples (n=9) and modern vegetation/O-horizon (Topsoil-PF) samples (n=9) from across the northeast Siberian Arctic.

Results show that these Topsoil-PF samples have higher %OC, higher OC/TN values, and more depleted $\delta^{13}C$-OC values than ICD-PF samples, suggesting that these former samples trace a fresher soil and/or vegetation source. Median concentrations of high-molecular weight *n*-alkanes (sum of C_{25}-C_{27}-C_{29}-C_{31}) were 210±350 µg/gOC (median±IQR) for Topsoil-PF and 250±81 µg/gOC for ICD-PF samples. Long-chain *n*-

The Cryosphere Discuss., doi:10.5194/tc-2017-17, 2017
Manuscript under review for journal The Cryosphere
Discussion started: 21 February 2017

alkanoic acids (sum of C_{22}-C_{24}-C_{26}-C_{28}) were more abundant than long-chain *n*-alkanes, both in Topsoil-PF samples (4700±3400 µg/gOC) and in ICD samples (6630±3500 µg/gOC). Whereas the two investigated sources differ on the bulk geochemical level, they are, however, virtually indistinguishable when using leaf wax concentrations and ratios.

However, on the molecular-isotope level, leaf wax biomarker δ^2H values are statistically different between Topsoil-PF and ICD-PF. The mean δ^2H value of C_{29} *n*-alkane was -246±13‰ (mean±stdev) for Topsoil-PF and -280±12‰ for ICD-PF, whereas the C_{31} *n*-alkane was -247±23‰ for Topsoil-PF and -297±15‰ for ICD-PF. The C_{28} *n*-alkanoic acid δ^2H value was -220±15‰ for Topsoil-PF and -267±16‰ for ICD-PF. With a dynamic isotopic range (difference between two sources) of 34 to 50‰, the isotopic fingerprints of individual, abundant, biomarker molecules from leaf waxes can thus serve as end-members to distinguish between these two sources. We tested this molecular δ^2H tracer along with another source-distinguishing approach, dual-carbon ($\delta^{13}C$-$\Delta^{14}C$) isotope composition of bulk OC, for a surface sediment transect in the Laptev Sea. Results show that general offshore patterns along the shelf-slope transect are similar, but the source apportionment between the approaches vary, which may highlight the advantages of either. The δ^2H molecular approach has the advantage that it circumvents uncertainties related to a marine end-member, yet the $\delta^{13}C$-$\Delta^{14}C$ approach has the advantage that it represents the bulk OC fraction thereby avoiding issues related to the molecular-bulk upscaling challenge. This study indicates that the application of δ^2H leaf wax values has potential to serve as a complementary quantitative measure of the source and differential fate of OC thawed out from different permafrost compartments.

The Cryosphere Discuss., doi:10.5194/tc-2017-17, 2017
Manuscript under review for journal The Cryosphere
Discussion started: 21 February 2017

1 Introduction

Climate warming is causing permafrost soils to thaw, exposing its organic matter (OM) to decomposition (e.g., Schuur et al., 2015; Zimov et al., 1993; Semiletov et al., 2012). Thaw will increase the hydrological connectivity of landscapes and will cause release of OM into the aquatic environment (Walvoord et al., 2012; Vonk et al., 2015; Anderson et al., 2011). Here, the OM can continue to decompose, generating greenhouse gases (e.g., Semiletov et al., 1996a,b; Anderson et al., 2009; Shakhova et al., 2015), or be destined for burial into inland and coastal sediments. These sedimentary archives serve as long- and short-term reservoirs that attenuate greenhouse gas emissions from thawing permafrost (Vonk and Gustafsson, 2013; Semiletov et al., 2011).

The release of OM from thawing permafrost into aquatic sediments varies over time and space. A recent study showed that at the end of the last glacial, the surface active layer of terrestrial permafrost released about 4.5 Tg organic carbon (OC) per year from just the Lena watershed onto the nearby shelf, whereas current annual OC release is estimated to be only about a tenth of this (Tesi et al., 2016). In addition to active layer material, OM from deeper and older permafrost sources can also thaw and be released into the environment (Shakhova et al., 2007, 2014). This process currently dominates the delivery of terrestrial material onto the East Siberian Arctic shelf (Vonk et al., 2012; Semiletov et al., 1999) and is expected to increase due to accelerating coastal erosion rates (Günther et al., 2013).

Different permafrost OC stocks exhibit variable vulnerabilities to thaw remobilization (Schuur et al., 2015). In addition to a subsea permafrost OC stock, soils and sediments of the terrestrial northern permafrost zone store about 1300±200 Pg OC, with separate upscaling approaches applied for soil stocks (0-3m depth), deltaic sediments (full depth) and Yedoma sediments (full depth) (Hugelius et al., 2014). Yedoma sediments, a.k.a. Ice Complex Deposits (ICD) are polygenetic, ice-rich Pleistocene-aged deposits that are present in the unglaciated parts of Siberia and Alaska (Schirrmeister et al., 2011). These deposits contain roughly a quarter of the OC stored in permafrost terrain, but estimates vary from ca. 200-400 Pg C (Strauss et al., 2013; Schuur et al., 2015). The presence of massive ice wedges in ICD causes landscapes to collapse upon thaw, exposing deeper stocks of OC. This type of relatively abrupt thaw is increasing in many parts of the arctic landscape (Schuur et al., 2015). At the same time, deepening of the active layer causes gradual thaw that occurs across entire landscapes (Shiklomanov et al., 2013).

With a tool to detect and monitor different types of permafrost OM in coastal environments, one could assess (historical and spatial) variability in permafrost source input, degradation and thaw, as well as the relative degradation of different permafrost types. For example, the relative release of OC from ICD versus topsoil permafrost has earlier been distinguished and quantified through the use of dual-carbon isotopes ($\delta^{13}C$ and $\Delta^{14}C$) on bulk OC in the shelf environment of the Laptev and East Siberian Sea. It was shown that topsoil permafrost OC dominates in suspended particulate matter (Karlsson et al., 2011; 2016; Vonk et al., 2012) and ICD

The Cryosphere Discuss., doi:10.5194/tc-2017-17, 2017
Manuscript under review for journal The Cryosphere
Discussion started: 21 February 2017

permafrost OC dominates in the surface sediments (Vonk et al., 2012; Semiletov et al., 2011; 2012). Vonk et al. (2014) further showed that topsoil OC is actively degraded during horizontal transport whereas ICD permafrost OC rapidly settles. Winterfeld et al. (2015) showed, using dual-carbon isotopes on riverine material, that suspended particulate OC in the Lena Delta mostly consists of Holocene material instead of material from ICD permafrost.

This $\delta^{13}C$-$\Delta^{14}C$ dual-carbon isotope approach carries the strong advantage that it operates on the bulk OC level, thereby circumventing the issues associated with molecular isotope proxies that relate to upscaling from the molecular to the bulk level (e.g. selective degradation, differences in physical association, dispersion differences). However, the $\delta^{13}C$-$\Delta^{14}C$ approach also has drawbacks, such as a weak distinction between the $\delta^{13}C$ end-member values of Topsoil-PF versus ICD-PF. Also, the marine $\delta^{13}C$ end member values in coastal Arctic shelf waters are uncertain and may be more depleted than at mid-latitudes due to uptake of relatively depleted dissolved CO_2 values caused by cold polar water (Meyers, 1997; Tesi et al. *this special issue*) or degradation of terrestrial matter (Anderson et al., 2009; 2011; Semiletov et al., 2013; 2016), generating a potential overlap between marine and topsoil $\delta^{13}C$ end-members.

Here we propose a complementary tool to trace permafrost OC release into the coastal environment based on molecular δ^2H analysis on leaf waxes. Isotopes in water molecules (δ^2H or $\delta^{18}O$) in glacial ice cores as well as in massive ground ice in the northern hemisphere have been used for reconstructing palaeotemperatures (Kotler and Burn, 2000; Johnson et al., 2001; Meyer et al., 2015) as the isotopic value of local precipitation is a function of local climate (Sachse et al., 2004; Smith and Freeman, 2006). Higher plants use water as their primary source of hydrogen during photosynthesis (Sternberg, 1988). The δ^2H isotope values of leaf wax *n*-alkanoic acids or *n*-alkanes are therefore reflecting the δ^2H isotopic value of local precipitation (e.g., Sachse et al., 2004; Sessions et al., 1999), after correction for the net fractionation during biosynthesis, and evapotranspiration (Leaney et al., 1985). Global precipitation values can vary by as much as 200‰ with values around 0‰ in the tropics but approaching -200‰ near the North Pole (www.iaea.org). Additionally, the fractionation between source water and plant wax molecules varies both in time and space, and can be up to -170‰ (Smith and Freeman, 2006; Sachse et al., 2004; Polissar and Freeman, 2010) but appears relatively small at higher latitudes (between -59 and -96‰; Shanahan et al., 2013; Wilkie et al., 2013; Porter et al., 2016). Differences in δ^2H signatures of leaf wax molecules from terrestrial regions with different (past) climates could therefore potentially be applied to derive the relative proportion of different types of thawing permafrost in nearby coastal settings. We hypothesize that δ^2H signatures of leaf wax *n*-alkanoic acids and *n*-alkanes are more depleted in OC from permafrost deposits formed during the colder and drier Pleistocene, compared to more enriched values in OC from active layer or surface permafrost formed during the warmer Holocene.

The Cryosphere Discuss., doi:10.5194/tc-2017-17, 2017
Manuscript under review for journal The Cryosphere
Discussion started: 21 February 2017

This study investigates a source-specific δ^2H signature for both ICD permafrost and recent, surface soil permafrost in Northeast Siberia. Furthermore, we explore the possibilities of using these isotopic end-member values in regional source-apportionment calculations that aim to quantify the relative contribution of different sources of permafrost OC. As permafrost thaw progresses, particularly in ice-rich permafrost such as ICD, it is increasingly important to trace the fate of remobilized and decomposing OC in the Arctic environment.

2 Methods

2.1 Sampling

A total of 18 samples were collected throughout the Siberian Arctic. Recent surface soils (n=7) and vegetation (n=2) samples were analyzed and (from here on) referred to as the "topsoil" permafrost (Topsoil-PF) sample set, whereas ICD-PF samples were obtained from ICD soil profiles (n=7) and suspended particulates from ICD formations (n=2) (Fig. 1 and Table 1). Eight offshore sediments along a shelf-slope-continental rise transect in the Laptev Sea were collected in 2014, further marine sampling details can be found in Bröder et al. (2016b).

The Topsoil-PF samples represent O and A soil genetic horizons in sites with active soil formation. The sites where chosen to represent typical soil and vegetation types in the investigated permafrost landscapes, including both taiga and tundra sites. Samples were collected by depth or soil horizon increments from open soil pits using fixed volume sampling procedures.

The ICD-PF samples were collected from vertical exposures that were excavated to expose intact permafrost. Fixed-volume samples were collected by coring horizontally into the frozen sediments to extract ICD-PF samples from consecutive depths.

For more details about sampling sites, including location, vegetation and soil types see table 1 (terminology following the U.S.D.A. Soil Taxonomy; Soil Survey Staff, 2014). Sampling was done in late summer near the time of maximum annual active layer depth, in July 2010 (CH DY-3A and 4A; Vonk et al. (2013)) and August 2011 (Palmtag et al., 2015) for the Kolyma River region, in August 2012 for the lower Lena River and Indigirka River (Siewert et al., 2015; Weiss et al., 2015) and in August 2013 for the upper Lena River (Siewert et al., 2016). For more detailed descriptions of sample collection we refer to these references. The vegetation samples CH Medv grass and CH Y4 grass were obtained from the tundra near Medvezhka River and a birch forest near Y4 stream, respectively, in July 2012.

Samples CH DY-3A and 4A were obtained in July 2010 at the Duvannyi Yar ICD exposure along the Kolyma River (Vonk et al., 2013). The particulate sediment samples were taken from thaw streams that were freshly formed from thawing ICD (transport time from thaw to sampling estimated to be less than 1h).

The Cryosphere Discuss., doi:10.5194/tc-2017-17, 2017
Manuscript under review for journal The Cryosphere
Discussion started: 21 February 2017

2.2 Analytical methods

Freeze-dried samples were extracted using an ASE 200 accelerated solvent extractor (Dionex Corporation, USA) using DCM/MeOH (9:1 v/v) at 80°C ($5x10^6$ Pa) (Wiesenberg et al., 2004). After the extraction, solvent-rinsed activated copper and anhydrous sodium sulfate were added to the extracts to remove sulfur and excess water, respectively. After 24 h, extracts were filtered on pre-combusted glass wool and concentrated with the rotary evaporator. Extracts were transferred into glass tubes, evaporated to complete dryness and re-dissolved in 500 µl of DCM. Lipid fractionation was performed via column chromatography using amino-propyl Bond Elut (500 mg/3 ml) to retain the acid fraction and Al_2O_3 to separate the hydrocarbon and polar fractions (Vonk et al., 2010).

Prior to the analyses, saturated *n*-alkanes (hydrocarbon fraction) were further purified using 10% $AgNO_3$ coated silica gel to retain the unsaturated fraction. The acid fraction was methylated using a mixture of HCl, MilliQ water and methanol at 80°C overnight to obtain the fatty acid methyl ester (FAME) fraction. Methylated acids were extracted with hexane and further purified using 10% $AgNO_3$ coated silica gel. The hydrocarbon and FAME fractions were quantified via gas chromatography mass spectrometry (GC–MS) in full scan mode (50-650 m/z) using the response factors of commercially available standards (Sigma-Aldrich). The GC was equipped with a 30 m×250 µm DB5-ms (0.25 µm thick film) capillary GC column. Initial GC oven temperature was set at 60°C followed by a 10°C min^{-1} ramp until a final temperature of 310°C (hold time 10 min).

The hydrogen-isotopic composition of hydrocarbon and FAME fractions was measured with continuous-flow GC - isotope ratio - MS. Purified extracts were concentrated and injected (1-2 µl) into a Thermo Trace Ultra GC equipped with a 30m×250 µm HP5 (0.25 µm thick film) capillary GC column. Oven conditions were similar to the setting used for the quantification. The conversion of organic biomarkers to elemental hydrogen was accomplished by high-temperature conversion (HTC) at 1420°C (Thermo GC Isolink). After the HTC, H_2 was introduced into the isotope ratio MS (Thermo Scientific™ Delta V™IRMS) for compound-specific determination of δ^2H values via a Thermo Conflo IV. Following a linearity test, we only used peaks with amplitude (mass 2) between 1500 and 8000 mV for the evaluation. The δ^2H values were calibrated against saturated HMW *n*-alkanes using the reference substance mix A4 (Biogeochemical Laboratories, Indiana University). The H3+ factor was determined every day and stayed constant (<3) throughout the evaluation. Each purified extract was injected three times. FAMEs were further corrected to account for the methylation agent by comparing the hydrogen abundance of lauric acid (C_{12}-FA; i.e. 12 carbon atoms) as acid and corresponding methyl ester. The average methylation effect for lauric acid was 23.97±3.9‰ (n=4). This factor was, normalized to chain length (i.e. increasing chain lengths result in lower corrections), applied to all the FAMEs. δ^2H values of *n*-alkanes and FAMEs are reported as mean, standard deviation and weighted average (Table 5).

The Cryosphere Discuss., doi:10.5194/tc-2017-17, 2017
Manuscript under review for journal The Cryosphere
Discussion started: 21 February 2017

253 ### 2.3 Source apportionment
254 The compound-specific δ^2H signatures in this study were used to differentiate
255 between the two major sources (end-members), Topsoil-PF and ICD-PF, using an
256 isotopic mass-balance model. We used a Markov chain Monte Carlo (MCMC) approach
257 to account for the end-member variability (Andersson et al., 2015; Bosch et al., 2015).
258 The end-members were represented by normal distributions, with mean and
259 standard deviations obtained from the literature values. For each Laptev Sea station,
260 the isotope signatures from three different terrestrial molecular markers (long-chain
261 *n*-alkanes C_{27}, C_{29} and C_{31}) were used jointly to improve source apportionment
262 precision. The δ^2H signatures for the two end-members were based on our Topsoil-
263 PF and ICD-PF samples (see Table 5 for mean source values).
264
265 The compound-specific δ^2H-based source apportionment was compared to
266 $\Delta^{14}C/\delta^{13}C$-based analysis of bulk OC using analogous MCMC techniques (e.g., Vonk et
267 al., 2012). The $\Delta^{14}C/\delta^{13}C$-approach allows estimation of the relative contribution of a
268 third source, marine, which does not affect the presently investigated (terrestrial)
269 compounds. Accounting for the marine component to OC allows direct comparison of
270 the Holocene and Pleistocene contributions. All MCMC calculations were made using
271 Matlab scripts (ver. 2014b) using 200,000 iterations, a burn-in phase (initial search
272 period) of 10,000 and a data thinning of 10.
273
274 The spatial extent of ICD in the Lena River Basin was calculated by overlaying
275 the extent of the drainage basin (from WRIBASIN: Watersheds of the World
276 published by the World Resources Institute, www.wri.org/publication/watersheds-
277 world) with the extent of the Yedoma Region (digitized from Romanovsky, 1993) in
278 an equal area map projection. It was assumed that 30% of the Yedoma Region consists
279 of intact ICD (following Strauss et al., 2013).
280
281 ## 3 Results
282
283 ### 3.1 Bulk geochemistry
284 The investigated Topsoil-PF and ICD-PF samples are, on a bulk geochemical level,
285 very different. Mean organic carbon contents (as %OC) and total nitrogen content (as
286 %TN) are 25±12 and 1.1±0.67 for Topsoil-PF samples, and 1.6±0.31 and 0.17±0.058
287 for ICD-PF samples, respectively (Table 1). This gives TOC/TN ratios of 25±8.0 for
288 Topsoil-PF samples and 10±2.6 for ICD-PF samples. Stable carbon isotopic values of
289 Topsoil-PF and ICD-PF samples are -27.8±1.3‰ and -25.7±0.75‰, respectively
290 (Table 1).
291
292 ### 3.2 Molecular geochemical composition
293 Long-chain *n*-alkanes and *n*-alkanoic acids are abundant in epicuticular waxes and
294 therefore indicative for a source of higher plants (Eglinton and Hamilton, 1967).
295 Concentrations of individual long-chain *n*-alkanes in Topsoil-PF samples ranged from
296 1 to 340 µg/gOC (C_{21}-C_{33}; Table 2) with an average chain length of 28±1.6. The sum
297 of high-molecular weight (HMW) *n*-alkanes (>C_{21}) was 420±330 µg/gOC

The Cryosphere Discuss., doi:10.5194/tc-2017-17, 2017
Manuscript under review for journal The Cryosphere
Discussion started: 21 February 2017

298 (median±IQR; interquartile range) and the most abundant *n*-alkanes added up to
299 210±350 µg/gOC (sum of C_{25}-C_{27}-C_{29}-C_{31}) (Table 4, Fig. 2a). For ICD-PF samples, the
300 individual concentrations of long-chain *n*-alkanes were between 4 and 160 µg/gOC,
301 and the average chain length 27±0.7 (Table 2). The sum of high-molecular weight *n*-
302 alkanes, and most abundant *n*-alkanes were 700±180 µg/gOC and 350±81 µg/gOC,
303 respectively (Table 4, Fig. 2a). The carbon preference index (CPI), a molecular ratio
304 indicative for degradation status with values >5 typical for fresher terrestrial material
305 and values approaching 1 typical for more degraded samples (Hedges and Prahl,
306 1993), showed values for Topsoil-PF samples of 7.3±3.6 (average±standard
307 deviation) and ICD-PF samples of 3.6±0.8 (CPI C_{23}-C_{31}; Table 4, Fig. 2c). The
308 $C_{25}/(C_{25}+C_{29})$ ratio, indicative for the input of peat moss (*Sphagnum sp.*) material
309 (Vonk and Gustafsson, 2009; *Sphagnum* values 0.72, higher plants 0.07; Nott et al.,
310 2000) was 0.33±0.22 (average±standard deviation) and 0.34±0.05 for Topsoil-PF and
311 ICD-PF samples, respectively (Table 4).
312
313 Long-chain *n*-alkanoic acids (C_{22} and above) were abundant in concentrations
314 between 0.122 and 2670 µg/gOC for individual homologues in topsoils, with the sum
315 of HMW *n*-alkanoic acids (>C_{22}) being 6400±4300 µg/gOC (median±IQR) and the
316 most abundant *n*-alkanoic acids (sum of C_{22}-C_{24}-C_{26}-C_{28}) adding up to 4700±3400
317 µg/gOC (Table 2, 4 and Fig. 2b). ICD-PF samples contained individual long-chain *n*-
318 alkanoic acids in 2.17 and 18700 µg/gOC (Table 3), a sum of HMW *n*-alkanoic acids of
319 8300±5100 µg/gOC, and the sum of most abundant, even *n*-alkanoic acids of
320 6600±3500 µg/gOC (Table 4). Topsoil-PF and ICD-PF samples had average chain
321 lengths of 24.1±1.1 and 24.3±0.59, and CPI (C_{22}-C_{28}) values of 5.9±2.7
322 (average±standard deviation) and 5.0±1.6, respectively (Table 4). Shorter-chain *n*-
323 alkanoic acids C_{16} and C_{18} are produced in basically all types of life in soils or aquatic
324 environments, and are not specific for higher plants. Topsoil-PF contained C_{16} and C_{18}
325 homologues in concentrations between 220 and 4600 µg/gOC, and ICD-PF samples
326 between 200 and 10400 µg/gOC (Table 3).
327
328 Degradation of organic matter involves the loss of functional groups, e.g. the loss of
329 carboxylic acids (Meyers and Ishiwatari, 1993). A high ratio of HMW *n*-alkanoic acids
330 over HMW *n*-alkanes in a sample therefore implies a relatively fresh, less degraded,
331 status (i.e. relatively more functional groups present). For Topsoil-PF samples, the
332 HMW *n*-alkanoic acid/HMW *n*-alkane ratio varied between 5.6 and 25 with an
333 average value of 13±7.6, whereas ICD-PF samples varied between 7.6 and 140 with
334 an average value of 29±43 (Table 4, Fig. 2f).
335
336 **3.3 Molecular isotopic composition**
337 We measured δ^2H values in long-chain *n*-alkanes and *n*-alkanoic acids between -119
338 and -313‰ (Fig. 3, Table 5). Mean values for HMW *n*-alkanes (C_{25}-C_{27}-C_{29}-C_{31}) were
339 between -201 and -247‰ for Topsoil-PF samples and between -221 and -297‰ for
340 ICD-PF samples, with consistently lower δ^2H for longer chain lengths. For HMW *n*-
341 alkanoic acids (C_{22}-C_{24}-C_{26}-C_{28}) mean δ^2H values were between -203 and -236‰ for
342 Topsoil-PF samples and between -261 and -278‰ for ICD-PF samples (Table 5). The

The Cryosphere Discuss., doi:10.5194/tc-2017-17, 2017
Manuscript under review for journal The Cryosphere
Discussion started: 21 February 2017

decrease in δ^2H values with increasing chain length is less distinct for *n*-alkanoic acids but one can observe a decrease of around 25-30‰ from C_{22} to C_{26} (Fig. 3). For ICD-PF samples, it seems that the isotopic depletion for the average of the three most abundant *n*-alkanes is comparable to the average for *n*-alkanoic acids, whereas in Topsoil-PF samples, the isotopic depletion for the three most abundant *n*-alkanes is a bit larger than for *n*-alkanoic acids (Fig. 4).

4 Discussion

4.1 Using bulk geochemistry and molecular proxies

Bulk geochemical and isotopic analysis, as well as analysis of molecular proxies remained inconclusive in distinghuishing between the two investigated sources in this study. Topsoil-PF samples have a higher organic content, higher TOC/TN values (representing fresh, higher plant material; Meyers, 1994) and more depleted $\delta^{13}C$ values (indicative for terrestrial C3 plants; Meyers, 1997) than ICD-PF samples, suggesting that these samples indeed trace a fresh soil and/or vegetation source (Table 1). The $\delta^{13}C$ values of a larger ICD-PF and Topsoil-PF dataset have earlier been summarized (Vonk et al., 2012 and references therein; Schirrmeister et al., 2011) giving values of -26.3±0.67‰ (n=374) and -28.2±2.0‰ (n=30), respectively. Our values (Table 1) are in a similar range. Despite the differences between these two sources in their bulk geochemistry, it is hard to use these parameters for source distinction as their variability is fairly high, and their behavior in the environment is not conservative, but e.g. affected by degradation processes. On a molecular geochemical level the two investigated sources are virtually indistinguishable as there is a considerable variation in molecular concentrations and proxy values (Fig. 2). Only one of the tested parameters, the CPI C_{23}-C_{31} of *n*-alkanes, showed a statistically significantly different value for the two investigated sources.

4.2 Evaluation of molecular δ^2H values as a source end-member

To alleviate the difficulty to distinguish between Topsoil-PF and ICD-PF with just bulk and molecular geochemical characteristics, we explore the δ^2H values of leaf wax molecules (i.e. long chain *n*-alkanoic acids and *n*-alkanes) to differentiate between their relative source contributions. The overall mean δ^2H of the four most abundant *n*-alkanoic acids is -231±29‰ and -271±13‰ for Topsoil-PF and ICD-PF samples, respectively. These values compare well with available literature (Fig. 5). Pautler et al. (2014) measured δ^2H values on C_{29} *n*-alkanes in modern soils of the Yukon, Canada of -252±9.1‰ (n=4) and aged soil δ^2H values of -269±8.6‰ (n=13; 24-25 ^{14}C-ka ago) and -273±16.4‰ (n=9; for MIS 4, ~70 ^{14}C-ka ago). Yang et al. (2011) also reported C_{29} *n*-alkane δ^2H values for modern vegetation from Alaska and Arctic Canada with an average value of -252±43‰ (n=8). Zech et al. (2011) reported values of C_{29} *n*-alkanes collected from a permafrost exposure along the Tumara River in northeast Siberia, with an average value of -266±7.5‰ (n=23) for glacial paleosoils and -247±9.4‰ (n=17) for interglacial paleosoils. Our values for C_{29} *n*-alkanes for Topsoil-PF (-246±13‰; n=9) and ICD-PF (-280±12‰; n=9) are in a similar range (Fig. 5). For C_{28} *n*-alkanoic acids, Wilkie et al. (2013) measured -252±8.7‰ (n=6) for modern

The Cryosphere Discuss., doi:10.5194/tc-2017-17, 2017
Manuscript under review for journal The Cryosphere
Discussion started: 21 February 2017

388 vegetation in northeast Siberia, whereas Porter et al. (2016) measured -269±2.7‰
389 (n=7) for ca. 31 cal ka BP old soils in the Yukon. Compared to these studies, our values
390 for C_{28} *n*-alkanoic acids are somewhat more enriched for Topsoil-PF with -220±15‰
391 (n=7) but roughly in the same range for ICD-PF with -267±16‰ (n=9).
392
393 The mean isotopic difference between the most abundant *n*-alkanoic acids of the two
394 investigated sources is around 40‰ (δ^2H values of -231±29‰ and -271±13‰ for
395 Topsoil-PF and ICD-PF samples, respectively). Despite the relatively large standard
396 deviations, the isotopic differences are statistically significant for each of the *n*-
397 alkanoic acids individually (C_{22}, C_{24}, C_{26}, C_{28}; Fig. 3). The isotopic differences between
398 the two sources for the mean value of the four most abundant *n*-alkanes is 35‰, with
399 a mean value of -229±33‰ and -264±34‰ for Topsoil-PF and ICD-PF samples,
400 respectively. Here, the individual *n*-alkane isotopic signatures are statistically
401 significantly different for C_{27}, C_{29}, C_{31} (Fig. 3) in Topsoil-PF and ICD-PF samples. The
402 selection and application of individual chain length δ^2H values as end-members, in
403 contrast to mean chain length values, might be more appropriate for several reasons;
404 (i) to reduce variability (δ^2H ranges for C_{29} and C_{31} *n*-alkanes and C_{22} and C_{24} *n*-
405 alkanoic acids are relatively low; Fig. 3), (ii) to target the most abundant species (C_{29}
406 and C_{31} *n*-alkanes are generally more abundant in soils and ICD-PF compared to
407 shorter chain lengths; Table 2), and (iii) to make use of the largest dynamic range
408 between source end-member values (C_{31} *n*-alkane δ^2H values of Topsoil-PF and ICD-
409 PF differ by 50‰). Based on these arguments, the C_{28} *n*-alkanoic acid and the C_{29} or
410 C_{31} *n*-alkanes are most appropriate to use for source-apportionment. The available
411 previous studies (Fig. 5) have also selected these chain lengths (C_{28} *n*-alkanoic acid
412 and C_{29} *n*-alkanes) for proxy development.
413
414 The use of molecular δ^2H values as tracers of terrestrial material in a marine or
415 coastal setting has the advantage that it avoids uncertainty issues related to definition
416 of the marine end-member. On the other hand, the inherent bulk-upscaling challenge
417 of any molecular proxies, is a disadvantage of the δ^2H approach as it introduces
418 unknowns related to the molecular-bulk upscaling effort (e.g. taking into account
419 sorting and recalcitrance; discussed in depth in 4.3). We also want to emphasize that
420 δ^2H leaf wax values in the two studied end-member sets (Topsoil-PF vs. ICD-PF)
421 largely depend on the climate (warm vs. cold) and continentality (near the coast vs.
422 further inland) during plant formation, and associated differences in fractionation
423 mechanisms. Consequently, when δ^2H values in samples are used for source-
424 apportionment, this may represent the fraction leaf wax produced in cold vs. warm
425 conditions (as well as degree of continentality), and not necessarily the fraction
426 Topsoil-PF vs. ICD-PF.
427
428 **4.3 Comparison with ^{13}C-^{14}C source-apportionment: a case-study**
429 Bulk OC dual-carbon isotope data provide a quantitative apportionment tool to assess
430 the relative contributions of Topsoil-PF vs. ICD-PF. Here, we present a case-study of
431 a shelf-slope transect in the Laptev Sea (Fig. 1) where both these source-
432 apportionment tools for the first time can be applied, compared and evaluated. The

The Cryosphere Discuss., doi:10.5194/tc-2017-17, 2017
Manuscript under review for journal The Cryosphere
Discussion started: 21 February 2017

shelf-slope transect of eight surface sediment samples stretches over 600 km from the nearshore zone (72.7°N, <10m water depth) to the continental rise (78.9°N, >3000m depth) (Table 6). More molecular and bulk geochemical characteristics of these samples can be found in Bröder et al. (2016b).

The $\delta^{13}C$-$\Delta^{14}C$ source-apportionment uses three end-members (marine, Topsoil-PF, and ICD-PF). End-member values are based on previously published values (Tesi et al., 2016); with a $\delta^{13}C$ value of -27.0±1.2‰ (n=38; Rodionow et al., 2006; Tesi et al., 2014; Gundelwein et al., 2007; Bird et al., 2002) for Topsoil-PF, and -26.3±0.67‰ (n=374; Vonk et al., 2012; Schirrmeister et al., 2011) for ICD-PF. The Topsoil-PF $\Delta^{14}C$ endmember was defined as -232±147‰ (n=29; Winterfeld et al., 2015; Jasinski et al., 1998; Kaiser et al., 2007; Höfle et al., 2013; Palmtag et al., 2015). For ICD-PF we used a $\Delta^{14}C$ value of -940±84‰ (n=300; Vonk et al., 2012 and references therein). The marine end-member value was -21.0±2.6‰ (n=10; Panova et al., 2015) and -50.4±12‰ (n=10; Panova et al., 2015) for $\delta^{13}C$ and $\Delta^{14}C$, respectively. Calculations were made using a Markov chain Monte Carlo approach (see 2.3).

For $\delta^{2}H$ source-apportionment there is no need to include a marine end-member as marine organisms do not produce long-chain *n*-alkanes or *n*-alkanoic acids. We were unfortunately only able to analyze *n*-alkanes in the shelf-slope transect samples, and no *n*-alkanoic acids, due to limitations in sample volume. We used the $\delta^{2}H$ values of the C_{27}, C_{29} and C_{31} *n*-alkanes, individually. In other words, these three chain lengths are taken as independent markers, providing an overdetermined system (i.e. two sources defined with three different markers). This is more representative than using the average (concentration-weighted) $\delta^{2}H$ value for these *n*-alkanes as the end-member values for each chain length are different. For Topsoil-PF we used -215±39‰, -246±13‰, and -247±23‰ for C_{27}, C_{29} and C_{31} *n*-alkanes, and for ICD-PF we applied -259±18‰, -297±15‰, and -282±13‰ for C_{27}, C_{29} and C_{31} *n*-alkanes, respectively (see also Table 5). Afterwards, we averaged the three end-member contributions derived from the three calculations for each station, thereby taking the variability introduced by the end-members into account.

The source apportionment of OC from Topsoil-PF and ICD-PF to surface sediments along the Laptev Sea transect differ between the bulk $\delta^{13}C$-$\Delta^{14}C$ and leaf wax $\delta^{2}H$ approaches (Table 6). The former approach suggests Topsoil-PF contributions between 21-70%, generally decreasing offshore, and, consequently, ICD-PF contributions of 30-79%, generally increasing offshore. The latter (leaf wax $\delta^{2}H$) approach results in a more extreme division of sources with Topsoil-PF contributions of 83-91% and ICD-PF contributions of 9-17%, with similar patterns nearshore and offshore (Table 6). A contribution of 9-17% may seem more in line with the estimated extent of ICD in the Lena River basin: 12% of the basin falls within the Yedoma Region (as defined by Romanovsky, 1993) and about 3% consists of intact ICD (see section 2.3). However, the cross-shelf sites are also strongly influenced by coastal and/or subsea erosion (Karlsson et al. 2011; Vonk et al., 2012; Semiletov et al., 2012; 2016) so the catchment characteristics are only one part of the story. It is challenging to

478 interpret the differences between the two proxies but we elaborate below on
479 potential reasons.
480
481 Assumptions in the bulk $\delta^{13}C$-$\Delta^{14}C$ approach may affect these results. First, the
482 outcome of the bulk $\delta^{13}C$-$\Delta^{14}C$ approach is sensitive to the definition of the marine
483 end-member. Changes in the currently used $\delta^{13}C$ and $\Delta^{14}C$ value of the marine end-
484 member of the East Siberian Arctic Shelf (n=10; Panova et al., 2015) would likely alter
485 the relative Topsoil-PF and ICD-PF contributions. The currently used standard
486 deviation for the $\delta^{13}C$ marine end-member is 2.6‰, which is much higher than the
487 values for the terrestrial end-members. Second, lateral transport time enroute the
488 shelf-slope transect (>600 kilometers) causing potentially significant aging of
489 sediments and its organic carbon is not accounted for in the source-apportionment.
490 Lateral transport time results in older surface OC ages on the shelf, compared to those
491 at the initial coastal deposition. Without correcting for this factor, the source-
492 apportionment will generate lower contributions of the (younger) Topsoil-PF
493 component. In an attempt to estimate this effect, we recalculated (similar to Bröder
494 et al. 2016a) the relative source contributions of Topsoil-PF, ICD-PF (and marine)
495 with the bulk $\delta^{13}C$-$\Delta^{14}C$ approach with the assumption that the Topsoil-PF ^{14}C age
496 would be subject to a cross-shelf lateral transport time of 5000 yrs. We assumed a
497 linear aging along the transect based on distance from the coast, with a maximum
498 value of 5000 yrs aging at station SW-01. This resulted in Topsoil-PF contributions
499 that were up to 20% higher (for the deepest stations) compared to the source-
500 apportionment where lateral transport time was unaccounted for (Table 6; Fig. 6).
501
502 Assumptions in the leaf wax $\delta^{2}H$ source-apportionment approach could potentially
503 also impact the outcomes, and hence differences with the bulk $\delta^{13}C$-$\Delta^{14}C$ results. First,
504 there is an inherent assumption related to the molecular to bulk level upscaling
505 challenge. We assume that the physical association of *n*-alkanes in different source
506 end-members (Topsoil-PF vs. ICD-PF) as well as their fractionation in the coastal
507 system is similar. However, previous research has shown that *n*-alkanes behave
508 rather differently upon their release into coastal waters; *n*-alkanes originating from
509 surface soil or vegetation debris are not bound to minerals and remain in suspension
510 during transport while being actively degraded, whereas *n*-alkanes originating in
511 deeper mineral soils settle quickly and are protected from extensive degradation
512 (Vonk et al., 2010). It is possible that most of the *n*-alkanes in the Laptev Sea sediment
513 transect originate in (deeper) mineral soils. An effect of physical association, as well
514 as the potential effect of hydrodynamic sorting patterns (Tesi et al., 2016) on the leaf
515 wax $\delta^{2}H$ values of both sources could impact the source-apportionment. Another
516 factor that can introduce a bias in our leaf wax $\delta^{2}H$ approach is a proton exchange of
517 the C-bound H-atoms in *n*-alkanes with environmental water. Although there is no
518 evidence for such exchange in young (<1 million years), cold sediments (Sessions et
519 al., 2004) this process could be enhanced in environments of low pH. The precise
520 effect of such exchange on the $\delta^{2}H$ signal of our samples (or end-members) is
521 unknown, but we suspect this process may be minimal.
522

The Cryosphere Discuss., doi:10.5194/tc-2017-17, 2017
Manuscript under review for journal The Cryosphere
Discussion started: 21 February 2017

When accounting for an estimated lateral transport time, the difference in estimates of source contribution by the two different approaches (bulk $\delta^{13}C$-$\Delta^{14}C$ and leaf wax $\delta^{2}H$) increases offshore, from about a 25% difference near the coast to a 40% difference at stations SW-01 and SW-03. This increasing offset between the results of the two end-member mixing methods may be caused by several factors such as variability in the marine end-member (e.g. due to changes in seasonal ice cover), a selective degradation (of the topsoil OC) enroute that introduces a source bias or isotopic fractionation, or remaining factors related to the lateral transport time (incorrect assumption of 5000 years, non-linear aging along transect). These differences highlight that both source-apportionment tools still could be fine-tuned further by (i) increasing the sample size of sources to reduce end-member uncertainties, (ii) continuous adjustments in end-member values and Markov chain Monte Carlo calculations based on latest knowledge, and (iii) assuring regional testing and verification of the method when applied to new environments.

5 Conclusions

Leaf wax $\delta^{2}H$ values in samples from aquatic recipient environments can be used to source-apportion the incoming terrestrial OC into two end-members; a Pleistocene ICD permafrost source and a younger, Holocene, topsoil source. Mean isotopic values of the C_{29} *n*-alkane, C_{31} *n*-alkane, and C_{28} *n*-alkanoic acid showed a dynamic, statistically significant range of 34, 50 and 46‰ between Topsoil-PF and ICD-PF samples, respectively, with ICD-PF samples being consistently more depleted indicative of formation during the colder and drier Pleistocene.

A case-study where we tested two isotopic proxies (leaf wax $\delta^{2}H$ and bulk $\delta^{13}C$-$\Delta^{14}C$) to calculate the relative terrestrial source contribution of Topsoil-PF and ICD-PF along a Laptev Sea surface sediment transect, showed that the two proxies yield variable results but overall generate similar trends offshore. We reason that variability is caused by factors such as lateral transport time, remaining uncertainties in end-member definition, or environmental factors such as physical association.

Both methods (leaf wax $\delta^{2}H$ and bulk $\delta^{13}C$-$\Delta^{14}C$) bring along their inherent disadvantages and advantages. The molecular approach has the distinct advantage that it circumvents the uncertainties that are associated with marine end-member definition in the case of bulk OC mixing model analysis. However, application of molecular $\delta^{2}H$ in source-apportionment studies brings along challenges related to the molecular-bulk upscaling step. Bulk $\delta^{13}C$-$\Delta^{14}C$ source-apportionment, on the other hand, has the advantage to operate on a bulk and perhaps more representative level, but is hampered by remaining uncertainties associated with the marine end-member.

This study shows that $\delta^{2}H$ of leaf wax molecules has the potential to be used in quantitative source-apportionment studies of thawing permafrost in coastal or marine settings. It can serve as an alternative or complementary approach to the commonly applied bulk $\delta^{13}C$-$\Delta^{14}C$ method. We recommend continuing optimization

of end-member definition and calibration in order to increase our understanding of the fate of thawing permafrost in the coastal environment.

Data availability

All data are available in Tables 1 through 6, as well as Supplementary Table S1.

Acknowledgements

We would like to acknowledge Robert Spencer, Sergey Davydov, Anya Davydova, Ekatarina Bulygina, Peter Kuhry, Matthias Siewert, Juri Palmtag, Niels Weiss, Martin Kruså, Volker Brüchert, Pete Hill, Vladimir Mordukhovich, Alexander Charkin, Deniz Kosmach, Per Andersson, and sampling crew and personnel of IB Oden and RV Yakob Smirnitskyi for help with sample collection in the field. Financial support has been provided by the Dutch NWO (Veni #863.12.004), US-NSF (Polaris Project #1044610), the Bolin Centre for Climate Research, the Knut and Alice Wallenberg Foundation (SWERUS-C3 Program; KAW #2011.0027), the Swedish Research Council (VR #621-2004-4039 and 621-2007-4631), the Russian Government (mega-grant under contract #14.Z50.31.0012 to I. S.), the Russian Science Foundation (#15-17-20032 to O. D.), the Nordic Council of Ministers Cryosphere-Climate-Carbon Initiative (project Defrost, #23001), the European Research Council (ERCAdG project CC-TOP #695331 to Ö.G.). This study was supported by the Delta Facility of the Faculty of Science, Stockholm University. GH would like to acknowledge funding from ESF-CryoCarb and EU FP7-PAGE21 projects for topsoil and ICD sample collection.

Author contributions

Land-based samples were collected by GH and JEV, ship-based samples were collected by IS, OD, ÖG, TT, LB, and JEV. Laboratory analysis was performed by LB, TT, and HH. Markov chain Monte Carlo simulations were run by AA. The manuscript was written by JEV with input of all co-authors.

References

Anderson, L. G., Jutterström, S., Hjalmarsson, S., Wåhlström, I., and Semiletov, I.P.: Out-gassing of CO_2 from Siberian Shelf seas by terrestrial organic matter decomposition, Geophys. Res. Lett. 36, L20601, doi:10.1029/2009GL040046, 2009.

Anderson, L.G., Björk, G., Jutterström, S., Pipko, I., Shakhova, N. Semiletov, I. and Wåhlström, I.: East Siberian Sea, an Arctic region of very high biogeochemical activity, Biogeosciences, 8, 1745-1754, doi:10.5194/bg-8-1745-2011, 2011.

Andersson, E., Deng, J., Du, K., Zheng, M., Yan, C., Sköld, M., and Gustafsson, Ö.: Regionally-varying combustion sources of the January 2013 severe haze events over Eastern China, Environ. Sci. Technol. 49(4), 2038-2043, doi: 10.1021/es503855e.

Bird, M. I., Santruckova, H., Arneth, A., Grigoriev, S., Gleixner, G., Kalaschnikov, Y. N., Lloyd, J., and Schulze, E.-D.: Soil carbon inventories and carbon-13 on a latitude transect in Siberia, Tellus, 54B, 631-641, 2002.

Bröder, L., Tesi, T., Salvado, J.A., Semiletov, I.P., Dudarev, O.V., and Gustafsson, Ö.:

612 Fate of terrigenous organic matter across the Laptev Sea from the mouth of the
613 Lena River to the deep sea of the Arctic interior, Biogeosciences 13, 5003, 5019.,
614 doi:10.5194/bg-13-5003-2016, 2016b.
615 Bröder, L., Tesi, T., Andersson, A., Eglinton, T.I., Semiletov, I.P., Dudarev, O.V., Roos,
616 P., and Gustafsson, Ö.: Historical records of organic matter supply and
617 degradation status in the East Siberian Sea, Org. Geochem. 91, 16-30,
618 doi:10.1016/j.orggeochem.2015.10.008, 2016a.
619 Bosch, C., Andersson, A., Kruså, M., Bandh, C., Hovorkova, I., Klanova, J., Knowles, T.
620 D. J., Pancost, R. D., Evershed, R. P., and Gustafsson, Ö.: Source apportionment of
621 polycyclic aromatic hydrocarbons in central European soils with compound-
622 specific triple isotopes ($\delta^{13}C$, $\Delta^{14}C$, and $\delta^{2}H$), Environ. Sci. Technol. 49(13), 7657-
623 7665, doi:10.1021/acs.est.5b01190.
624 Eglinton, G., and Hamilton, R.J.: Leaf epicuticular waxes, Science 156, 1322-1335,
625 1967.
626 Gundelwein, A., Mueller-Lupp, T., Sommerkorn, M., Haupt, E. T. K., Pfeiffer, E. M., and
627 Wiechmann, H.: Carbon in tundra soils in the Lake Labaz region of arctic Siberia,
628 Eur. J. Soil Sci., 58, 1164-1174.
629 Günther, F., Overduin, P.P., Sandakov, A.V., Grosse, G., and Grigoriev, M.N.: Short- and
630 long-term thermo-erosion of ice-rich permafrost coasts in the Laptev Sea region,
631 Biogeosciences, 10, 4297-4318, doi:10.5194/bg-10-4297-2013, 2013.
632 Hedges, J.I., and Prahl, F.G.: Early diagenesis: consequences for applications of
633 molecular biomarkers, in *Organic Geochemistry: principles and applications.* Engel,
634 M.H., and Macko, S.A. (ed.). Plenum Press, New York. pp 237-253, 1993.
635 Höfle, S., Rethemeyer, J., Mueller, C. W., and John, C.: Organic matter composition and
636 stabilization in a polygonal tundra soil of the Lena Delta, Biogeosciences, 10, 3145-
637 3158, doi:10.5194/bg-10-3145-2013, 2013
638 Hugelius, G. Strauss, J., Zubrzycki, S., Harden, J. W., Schuur, E. A. G., Ping, C.-L.,
639 Schirrmeister, L., Grosse, G., Michaelson, G. J., Koven, C. D., O'Donnell, J. A., Elberling,
640 B., Mishra, U., Camill, P., Yu, Z., Palmtag, J., and Kuhry, P.: Estimated stocks of
641 circumpolar permafrost carbon with quantified uncertainty ranges and identified
642 data gaps, Biogeosciences 11, 6573-6593, doi:10.5194/bg-11-6573-2014, 2014.
643 Jasinski, J. P. P., Warner, B. G., Andreev, A. A., Aravena, R., Gilbert, S. E., Zeeb, B. A., Smol,
644 J. P., and Velichko, A. A.: Holocene environmental history of a peatland in the Lena
645 River valley, Siberia, Can. J. Earth Sci., 35, 637-648, 1998.
646 Johnsen, S. J., Dahl-Jensen, D., Gundestrup, N., Steffensen, J. P., Clausen, H. B., Miller,
647 H.: Oxygen isotope and palaeotemperature records from six Greenland ice-core
648 stations: Camp Century, Dye-3, GRIP, GISP2, Renland and NorthGRIP, J. Quat. Sci.
649 16, 299-307, doi:10.1002/jqs.622, 2001.
650 Kaiser, C., Meyer, H., Biasi, C., Rusalimova, O., Barsukov, P., and Richter, A.:
651 Conservation of soil organic matter through cryoturbation in arctic soils in
652 Siberia, J. Geophys. Res.-Biogeosciences, 112, G2, doi:10.1029/2006JG000258,
653 2007.
654 Karlsson, E. S., Charkin, A., Dudarev, O., Semiletov, I., Vonk, J. E., Sanchez-Garcia, L.,
655 Andersson, A., and Gustafsson, O.: Carbon isotopes and lipid biomarker
656 investigation of sources, transport and degradation of terrestrial organic matter
657 in the Buor-Khaya Bay, SE Laptev Sea, Biogeosciences 8, 1865-1879,

doi:10.5194/bg-8-1865-2011, 2011.

Karlsson, E. S., Gelting, J., Tesi, T., van Dongen, B., Andersson, A., Semiletov, I., Charkin, Al., Dudarev, O., and Gustafsson, Ö.: Different sources and degradation state of dissolved, particulate, and sedimentary organic matter along the Eurasian Arctic coastal margin, Global Biogeochem. Cycles, 30, 898-919, doi:10.1002/2015GB005307.

Kotler, E., and Burn, C. R.: Cryostratigraphy of the Klondike "muck" deposits, westcentral Yukon Territory, Can. J. Earth Sci. 37, 849-861, doi:10.1139/e00-013, 2000.

Leaney, F. W., Osmond, C. B., Allison, G. B., and Ziegler, H.: Hydrogen-isotope composition of leaf water in C-3 and C-4 plants - its relationship to the hydrogen isotope composition of dry-matter, Planta 164 (2), 215-220.

Meyer, H., Opel, T., Laepple, T., Dereviagin, A.Y., Hoffmann, K., and Werner, M.: Long-term winter warming trend in the Siberian Arctic during the mid- to late Holocene, Nat. Geosci. 8, 122-125, doi:10.1038/ngeo2349, 2015.

Meyers P. A., Ishiwateri R.: Lacustrine organic geochemistry – an overview of indicators of organic matter sources and diagenesis in lake sediments, Org. Geochem. 20, 867-900, doi:10.1016/0146-6380(93)90100-P, 1993.

Meyers, P. A.: Preservation of elemental and isotopic source identification of sedimentary organic matter, Chem. Geol. 114, 289-302, doi:10.1016/0009-2541(94)90059-0, 1994.

Meyers, P. A.: Organic geochemical proxies of paleoceanographic, paleolimnologic and paleoclimatic processes, Org. Geochem. 27, 213-250, doi:10.1016/S0146-6380(97)00049-1, 1997.

Nott, C. J., Xie, S., Avsejs, L. A., Maddy, D., Chambers, F. M., Evershed, R. P.: *n*-Alkane distributions in ombotrophic mires as indicators of vegetation change related to climatic variation, Org. Geochem. 31, 231-235, doi:10.1016/S0146-6380(99)00153-9, 2000.

Palmtag J., Hugelius G., Lashchinskiy N., Tamstorf M.P., Richter A., Elberling B. and Kuhry, P. (2015) Storage, Landscape Distribution, and Burial History of Soil Organic Matter in Contrasting Areas of Continuous Permafrost, Arctic, Antarctic, and Alpine Research, 47(1), 71-88, doi: http://dx.doi.org/10.1657/AAAR0014-027

Polissar, P. J., and Freeman, K. H.: Effects of aridity and vegetation on plant-wax dD in modern lake sediments, Geochim. Cosmochim. Ac. 74, 5785-5797, doi:10.1016/j.gca.2010.06.018, 2010.

Panova, E., Tesi, T., Pearce, C., Salvado, J. A., Karlsson, E. S., Kruså, M., Semiletov, I. P., and Ö. Gustafsson: Geochemical compositional differences of the supramicron plantkont-dominated fraction in two regimes of the Marginal Ice Zone (MIZ) of the outer East Siberian Arctic Shelf, AGU Fall meeting 2015 abstract, 2015.

Pautler, B. G., Reichart, G.-J., Sanborn, P. T., Simpson, M. J., Weijers, J. W. H.: Comparison of soil derived tetraether membrane lipid distributions and plantwax dD compositions for reconstruction of Canadian Arctic temperatures, Palaeogeogr. Palaeoclimatol. Palaeoecol. 404, 78-88, doi:10.1016/j.palaeo.2014.03.038, 2014

703 Porter, T. J., Froese, D. G., Feakins, S. J., Bindeman, I. N., Mahoney, M. E., Pautler, B. G.,
704 Reichart, G.-J., Sanborn, P. T., Simpson, M. J., and Weijers, J. W. H.: Multiple water
705 isotope proxy reconstruction of exteremely low last glacial temperatures in
706 Eastern Beringia (Western Arctic), Quat. Sci. Rev. 137, 113-125,
707 doi:10.1016/j.quascirev.2016.02.006, 2016.
708 Rodionow, A., Flessa, H., Kazansky, O., and Guggenberger, G.: Organic matter
709 composition and potential trace gas production of permafrost soils in the forest
710 tundra in northern Siberia, Geoderma, 135, 49-62, 2006.
711 Romanovsky, N. N.: Fundamentals of the cryogenesis of the lithosphere. University
712 Press, Moscow, pp. 1-336 (in Russian), 1993.
713 Sachse, D., Radke, J., and Gleixner, G.: Hydrogen isotope ratios of recent lacustrine
714 sedimentary n-alkanes record modern climate variability, Geochim. Cosmochim.
715 Ac., 68, 4877–4889, doi:10.1016/j.gca.2004.06.004, 2004.
716 Schuur, E. A. G., McGuire, A. D., Schädel, C., Grosse, G., Harden, J. W., Hayes, D. J.,
717 Hugelius, G., Koven, C. D., Kuhry, P., Lawrence, D. M., Natali, S. M., Olefeldt, D.,
718 Romanovsky, V. E., Schaefer, K., Turetsky, M. R., Treat, C. C., and Vonk, J. E.:
719 Climate change and the permafrost carbon feedback, Nature, 250, 171-178,
720 doi:10.1038/nature14338, 2015.
721 Schirrmeister, L. Kunitsky, V. V., Grosse, G., Wetterich, S., Meyer, H., Schwamborn, G.,
722 Babiy, O., Derevyagin, A., and Siegert, C.: Sedimentary characteristics and origin of
723 the Late Pleistocene Ice Complex on north-east Siberian Arctic coastal lowlands
724 and islands – A review, Quatern. Int. 241, 3-25, doi:10.1016/j.quaint.2010.04.004,
725 2011.
726 Semiletov I.P., Pipko I.I., Shakhova N.E., Dudarev O.V., Pugach S.P., Charkin A.N., McRoy
727 C.P., Kosmach D., and Gustafsson, Ö: Carbon transport by the Lena River from its
728 headwaters to the Arctic Ocean, with emphasis on fluvial input of terrestrial
729 particulate organic carbon vs. carbon transport by coastal erosion, Biogeosciences,
730 8, 2407-2426, 2011.
731 Semiletov I.P., Shakhova N. E., Sergienko V.I., Pipko I.I., and O. Dudarev: On Carbon
732 Transport and Fate in the East Siberian Arctic Land-Shelf-Atmosphere System,
733 Environment Res. Lett., 7, doi:10.1088/1748-9326/7/1/015201, 2012.
734 Semiletov, I.P., Shakhova, N.E., Pipko, I.I., Pugach, S.P., Charkin, A.N., Dudarev, O.V.,
735 Kosmach, D.A., and S. Nishino (2013). Space-time dynamics of carbon and
736 environmental parameters related to carbon dioxide emissions in the Buor-Khaya
737 Bay of the Laptev Sea, Biogeosciences, 10, 5977-5996, doi:10.5194/bg-10-5977-
738 2013
739 Semiletov I., Pipko I., Gustafsson O., Anderson L., Sergienko V., Pugach S., Dudarev O.,
740 Charkin A., Broder L., Andersson A., Spivak E., and N. Shakhova (2016),
741 Acidification of the East Siberian Arctic Shelf waters through addition of
742 freshwater and terrestrial carbon, Nature Geoscience, doi:10.1038/NEGO 2695,
743 2016.
744 Semiletov I.P., Pipko, I.I., Pivovarov, N.Y., Popov, V. V., Zimov, S. A., Voropaev, Y. V.,
745 and S.P. Davydov: Atmospheric carbon emissions from northern lakes: a factor of
746 global significance, Atmospheric. Environment, 30, 1657-1671, 1996a.

Semiletov I.P., Pivovarov, N.Y., Pipko, I. I., Gukov, A. Y., Volkova, T. I., Sharp, J. P., Shcherbakov, Y. S., and K. P. Fedorov: Dynamics of dissolved CH_4 and CO_2 in the Lena River Delta and Laptev Sea. Transactions (Doklady) of the Russian Academy of Sciences, 350 (3), 401-404 (translated into English), 1996b.

Semiletov, I.P.: Destruction of the coastal permafrost ground as an important factor in biogeochemistry of the Arctic Shelf waters, Trans. (Doklady) Russian Acad. Sci., 368, 679-682 (translated into English), 1999.

Siewert, M.B., Hanisch, J., Weiss, N., Kuhry, P., Maximov, T.C., Hugelius, G.: Comparing carbon storage of Siberian tundra and taiga permafrost ecosystems at very high spatial resolution. Journal of Geophysical Research: Biogeosciences, 120, doi:10.1002/2015JG002999, 2015.

Siewert, M.B., Hugelius, G., Heim, B., Faucherre, S.: Landscape controls and vertical variability of soil organic carbon storage in permafrost-affected soils of the Lena River Delta. Catena, 147, 725–741. doi:10.1016/j.catena.2016.07.048, 2016.

Soil Survey Staff (2014), Keys to Soil Taxonomy, 12th ed., U.S. Department of Agriculture & Natural Resources Conservation Service, Washington, D. C.

Sessions, A. L., Burgoyne, T.W., Schimmelmann, A., and Hayes, J. M.: Fractionation of hydrogen isotopes in lipid biosynthesis, Org. Geochem., 30, 1193–1200, doi:10.1016/S0146-6380(99)00094-7, 1999.

Sessions, A.L., Sylva, S.P., Summons, R.E., and Hayers, J.M.: Isotopic exchange of carbon-bound hydrogen over geologic timescales, Geochim. Cosmochim. Ac. 68, 1545-1559, doi:10.1016/j.gca.2003.06.004, 2004.

Shakhova, N. and I. Semiletov: Methane release and coastal environment in the East Siberian Arctic shelf, Journal of Marine Systems, 66 (1-4), 227-243, 2007.

Shakhova, N., Semiletov, I., Leifer, I., , Sergienko, V., Salyuk, A., Kosmach, D., Chernikh D., Stubbs Ch., Nicolsky D., Tumskoy V., and O. Gustafsson: Ebullition and storm-induced methane release from the East Siberian Arctic Shelf, Nature Geoscience 7-1, 64-70, doi: 10.1038/NGEO2007, 2014.

Shakhova N., I. Semiletov, V. Sergienko, L. Lobkovsky, V. Yusupov, A. Salyuk, A. Salomatin, D. Chernykh, D. Kosmach, G. Panteleev, D. Nicolsky, V. Samarkin, S. Joye, A. Charkin, O. Dudarev, A. Meluzov, and Ö. Gustafsson: The East Siberian Arctic Shelf: towards further assessment of permafrost-related methane fluxes and role of sea ice. Phil. Trans. R. Soc. A, vol. 373: 20140451. doi:10.1098/rsta.2014.0451, 2015.

Shanahan, T.M., Hughen, K.A., Ampel, L., Sauer, P.E., and Fornace, K.: Environmental controls on the 2H/1H values of terrestrial leaf waxes in the eastern Canadian Arctic, Geochim. Cosmochim. Ac. 119, 286-301, doi:10.1016/j.gca.2013.05.032, 2013.

Shiklomanov, N. I., Streletskiy, D. A., Little, J. D., and Nelson, F. E.: Isotropic thaw subsidence in undisturbed permafrost landscapes, Geophys. Res. Lett. 40, 6356-6361, doi:10.1002/2013GL058295, 2013.

Smith, F.A., and Freeman, K.H.: Influence of physiology and climate on dD of leaf wax n-alkanes from C3 and C4 grasses, Geochim. Cosmochim. Ac. 70, 1172-1187, doi:10.1016/j.gca.2005.11.006, 2006.

791 Strauss, J., Schirrmeister, L., Grosse, G., Wetterich, S., Ulrich, M., Herzschuh, U., and
792 Hubberten, H.-W.: The deep permafrost carbon pool of the Yedoma region in
793 Siberia and Alaska. Geophys. Res. Lett. 40, 6165-6170,
794 doi:10.1002/2013GL058088, 2013.
795 Tesi, T., I. Semiletov, G. Hugelius, O. Dudarev, P. Kuhry, and Gustafsson, Ö.:
796 Composition and fate of terrigenous organic matter along the Arctic land-ocean
797 continuum in East Siberia: insights from biomarkers and carbon isotopes,
798 Geochim. Cosmochim. Acta, 133, 235-256, 2014.
799 Tesi, T., Semiletov, I., Dudarev, O., Andersson, A., and Gustafsson, Ö.: Matrix
800 association effects on hydrodynamic sorting and degradation of terrestrial organic
801 matter during cross-shelf transport in the Laptev and East Siberian shelf seas, J.
802 Geophys. Res.-Biogeosciences, 121, 731-752, doi:10.1002/2015JG003067, 2016a.
803 Tesi, T., Muschitiello, F., Smittenberg, R. H., Jakobsson, M., Vonk, J. E., Hill, P.,
804 Andersson, A., Kirchner, N., Noormets, R., Dudarev, O., Semiletov, I., and Gustafsson,
805 Ö.: Massive remobilization of permafrost carbon during post-glacial warming, in
806 review at Nature Communications, 2016b.
807 Vonk, J. E., van Dongen, B. E., and Gustafsson, Ö.: Selective preservation of old organic
808 carbon fluvially released from sub-arctic soils, Geophys. Res. Lett. 37, L11605,
809 2010
810 Vonk, J. E., Sanchéz-García, L., van Dongen, B. E., Alling, V., Kosmach, D., Charkin, A.,
811 Semiletov, I. P., Dudarev, O. V., Shakhova, N., Roos, P., Eglinton, T. I., Andersson, A.,
812 and Gustafsson, Ö.: Activation of old carbon by erosion of coastal and subsea
813 permafrost in Arctic Siberia, Nature, 489, 137–140, doi:10.1038/nature11392,
814 2012.
815 Vonk, J. E., and Gustafsson, Ö.: Permafrost-carbon complexities, Nat. Geosci. 6, 675-
816 676, doi:10.1038/ngeo1937, 2013.
817 Vonk, J. E., Mann, P. J., Davydov, S., Davydova, A., Spencer, R. G. M., Schade, J.,
818 Sobczak, W. V., Zimov, N., Zimov, S., Bulygina, E., Eglinton, T. I., and Holmes, R. M.:
819 High biolability of ancient permafrost carbon upon thaw, Geophys. Res. Lett., 40,
820 2689-2693, doi:10.1002/grl.50348, 2013.
821 Vonk, J. E., Semiletov, I. P., Dudarev, O. V., Eglinton, T. I., Andersson, A., Shakhova, N.,
822 Charkin, A., Heim, B., and Gustafsson, Ö.: Preferential burial of permafrost-derived
823 organic carbon in Siberian-Arctic shelf waters, J. Geophys. Res. Oceans 119, 8410-
824 8421, doi:10.1002/2014JC010261, 2014.
825 Vonk, J. E., Tank, S. E., Bowden, W. B., Laurion, I., Vincent, W. F., Alekseychik, P., Amyot,
826 M., Billet, M. F., Canario, J., Cory, R. M., Deshpande, B. N., Helbig, M., Jammet, M.,
827 Karlsson, J., Larouche, J., MacMillan, G., Rautio, M., Walter Anthony, K. M., and
828 Wickland, K. P.: Effects of permafrost thaw on Arctic aquatic ecosystems,
829 Biogeosciences 12, 7129-7167, doi:10.5194/bg-12-7129-2015, 2015.
830 Walvoord, M. A., Voss, C. I., and Wellman, T. P.: Influence of permafrost distribution
831 on groundwater flow in the context of climate-driven permafrost thaw: Example
832 from Yukon Flats Basin, Alaska, United States, Water Resour. Res. 48, W07524,
833 doi:10.1029/2011WR011595, 2012.
834 Weiss N, Blok D, Elberling B, Hugelius G, Jørgensen CJ, Siewert MB, Kuhry P:
835 Thermokarst dynamics and soil organic matter characteristics controlling initial
836 carbon release from permafrost soils in the Siberian Yedoma region. Sedimentary

837 Geology, http://dx.doi.org/10.1016/j.sedgeo.2015.12.004, 2015.
838 Wiesenberg, G., Schwark, L., Schmidt, M., 2004. Improved automated extraction and
839 separation procedure for soil lipid analyses. European Journal of Soil Science 55,
840 349-356.
841 Wilkie, K.M.K., Chapligin, B., Meyer, H., Burns, S., Petsch, S., and Brigham-Grette, J.:
842 Modern isotope hydrology and controls on dD of plant leaf waxes at Lake
843 El'gygytgyn, NE Russia, Clim. Past 9, 335-352, doi:10.5194/cp-9-335-2013, 2013.
844 Winterfeld, M., Lepple, T., and Mollenhauer, G.: Characterization of particulate
845 organic matter in the Lena River delta and adjacent nearshore zone, NE Siberia –
846 Part I: Radiocarbon inventories, Biogeosciences, 12, 3769-3788, doi:10.5194/bg-
847 12-3769-2015, 2015.
848 Yang, H., Liu, W., Leng, Q., Hren, M.T., and Pagani, M.: Variation in n-alkane dD values
849 from terrestrial plants at high latitude: implications for paleoclimate
850 reconstruction, Org. Geochem. 42, 283-288,
851 doi:10.1016/j.orggeochem.2011.01.006, 2011.
852 Zech, R., Huang, Y., Zech, M., Tarozo, R., and W. Zech: High carbon sequestration in
853 Siberian permafrost loess-paleosols during glacials, Clim. Past, 7, 501-509,
854 doi:10.5194/cp-7-501-2011, 2011.
855 Zimov, S.A., Semiletov, I. P. Daviodov, S. P., Voropaev, Y. V., Prosyannikov, S. F., Wong,
856 C. S., and Y.-H. Chan: Wintertime CO_2 emission from soils of Northeastern Siberia.
857 Arctic, 46, 197-204, 1993.
858

The Cryosphere Discuss., doi:10.5194/tc-2017-17, 2017
Manuscript under review for journal The Cryosphere
Discussion started: 21 February 2017

Figure 1
Map of coastal northeast Siberia showing the extent of ice complex permafrost (ICD; red) overlaid with the location of ice complex (n=9; black diamonds) and topsoil samples (n=9; green squares). The shelf-slope Laptev Sea transect is shown with yellow stars.

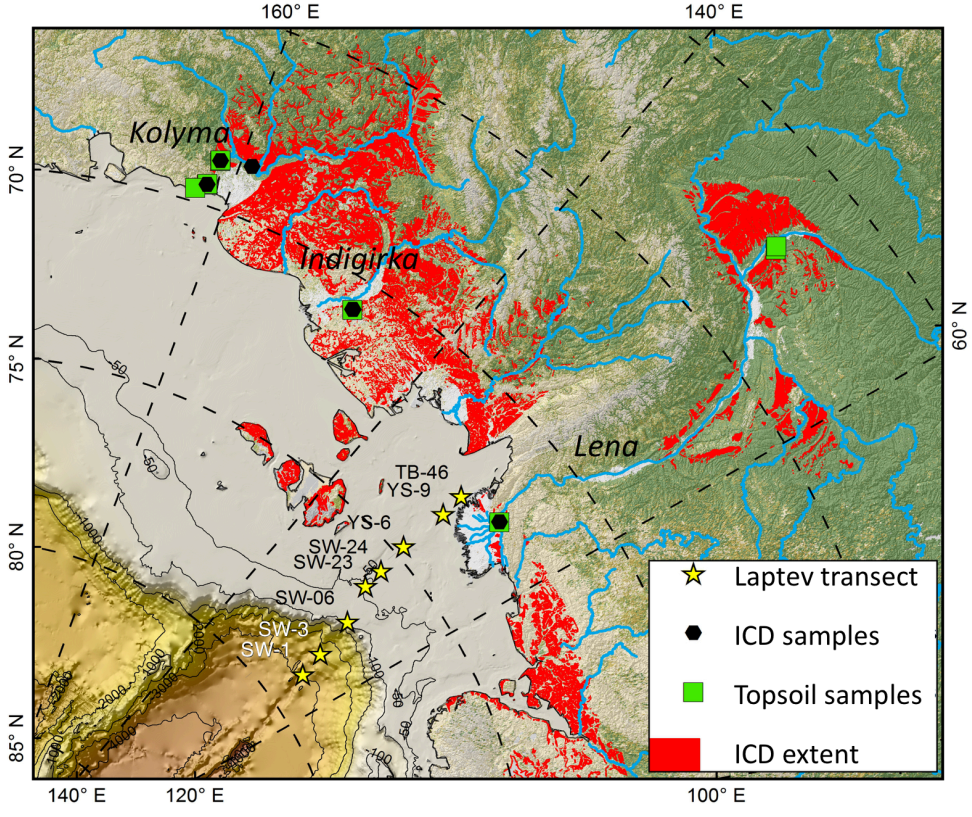

The Cryosphere Discuss., doi:10.5194/tc-2017-17, 2017
Manuscript under review for journal The Cryosphere
Discussion started: 21 February 2017

867 **Figure 2**
868 Molecular concentrations and ratios of topsoil Holocene permafrost (green) and deeper
869 Pleistocene permafrost (blue) samples, with (a) the sum of odd *n*-alkanes C_{25}-C_{31}, (b) the
870 sum of even *n*-alkanoic acids C_{22}-C_{28}, (C) the Carbon Preference Index (CPI) for *n*-
871 alkanes C_{23}-C_{31}, (d), the CPI for *n*-alkanoic acids C_{22}-C_{28}, (e) the ratio of C_{25} over
872 C_{25}+C_{29} *n*-alkanes, and (f) the sum of high-molecular weight (HMW) *n*-alkanoic acids
873 over HMW *n*-alkanes. The CPI is calculated as $CPI_{i\text{-}n} = ½ \Sigma (X_i+X_{i+2}+...+X_n)/ \Sigma (X_{i-1}+X_{i+1}+...+X_{n-1}) + ½ \Sigma (X_i+X_{i+2}+...+X_n)/ \Sigma (X_{i+1}+X_{i+3}+...+X_{n+1})$, where X is
874
875 concentration. Stars indicate that the two compared values are statistically significant
876 (95% confidence). Note that panel a and b are reported as median±IQR (interquartile
877 range) and the other panels are reported as average±standard deviation.
878

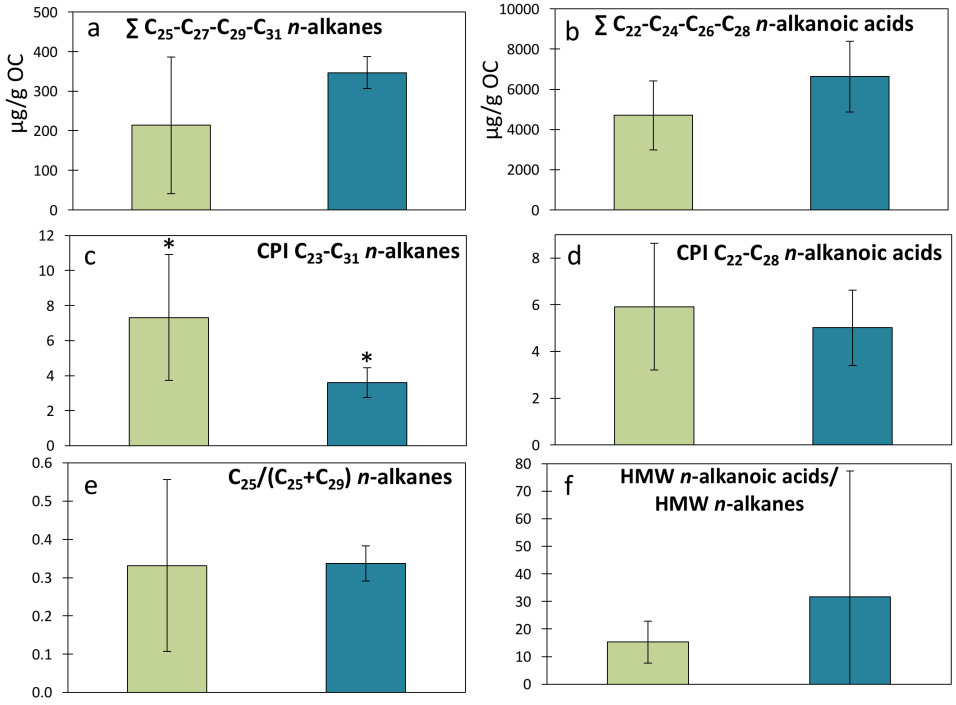

879
880

The Cryosphere Discuss., doi:10.5194/tc-2017-17, 2017
Manuscript under review for journal The Cryosphere
Discussion started: 21 February 2017

881 **Figure 3**
882 Molecular isotopic signature against chain length of long chain *n*-alkanoic acids (top) and
883 *n*-alkanes (bottom) for Holocene topsoil samples (green) and Pleistocene ice complex
884 samples (ICD; blue). Stars indicate that the two compared values are statistically
885 significant (95% confidence). Standard deviations are represented as vertical bars, and
886 are smaller than the sample circles when not visible.
887

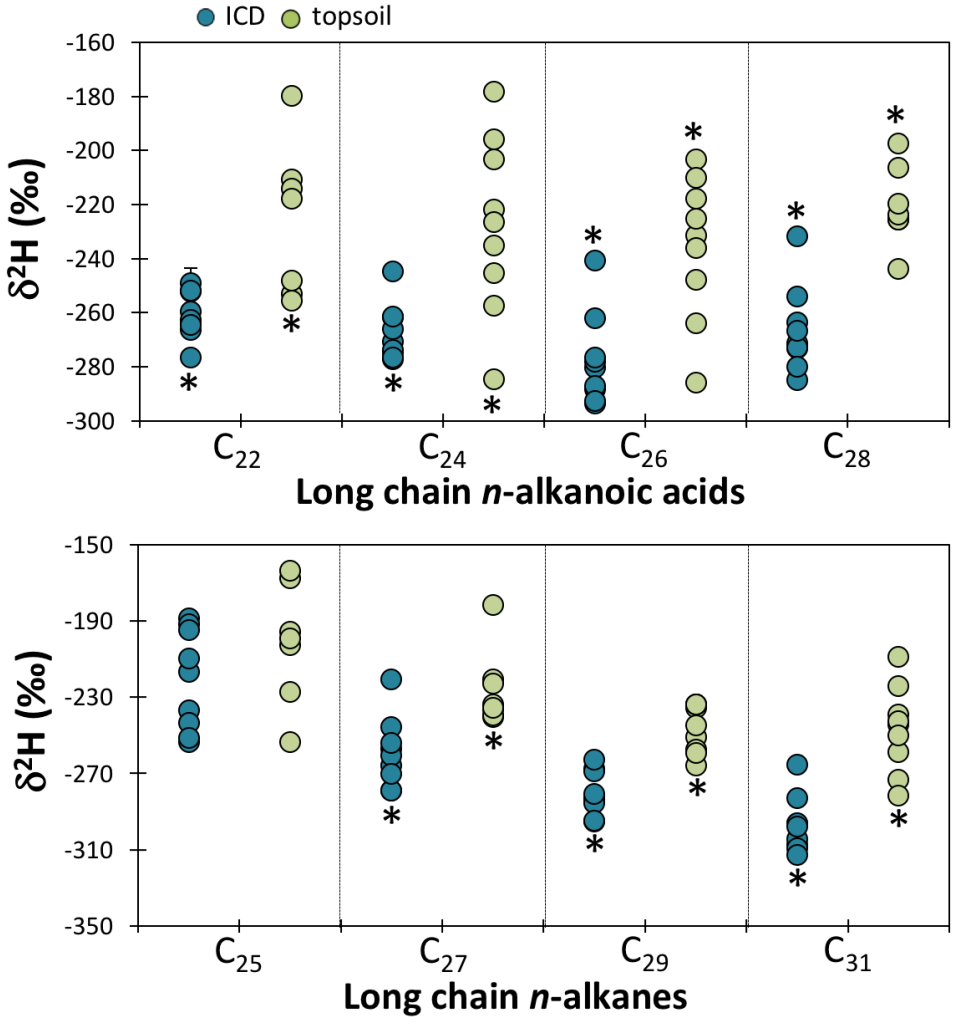

888
889
890
891
892

The Cryosphere Discuss., doi:10.5194/tc-2017-17, 2017
Manuscript under review for journal The Cryosphere
Discussion started: 21 February 2017

893 **Figure 4**
894 Concentration-weighted mean δ^2H values of C_{27}-C_{29}-C_{31} *n*-alkanes plotted against
895 concentration-weighted mean δ^2H values of C_{24}-C_{26}-C_{28} *n*-alkanoic acids to illustrate the
896 fractionation differences between these two leaf wax markers. Dashed line indicates an
897 identical fractionation.
898

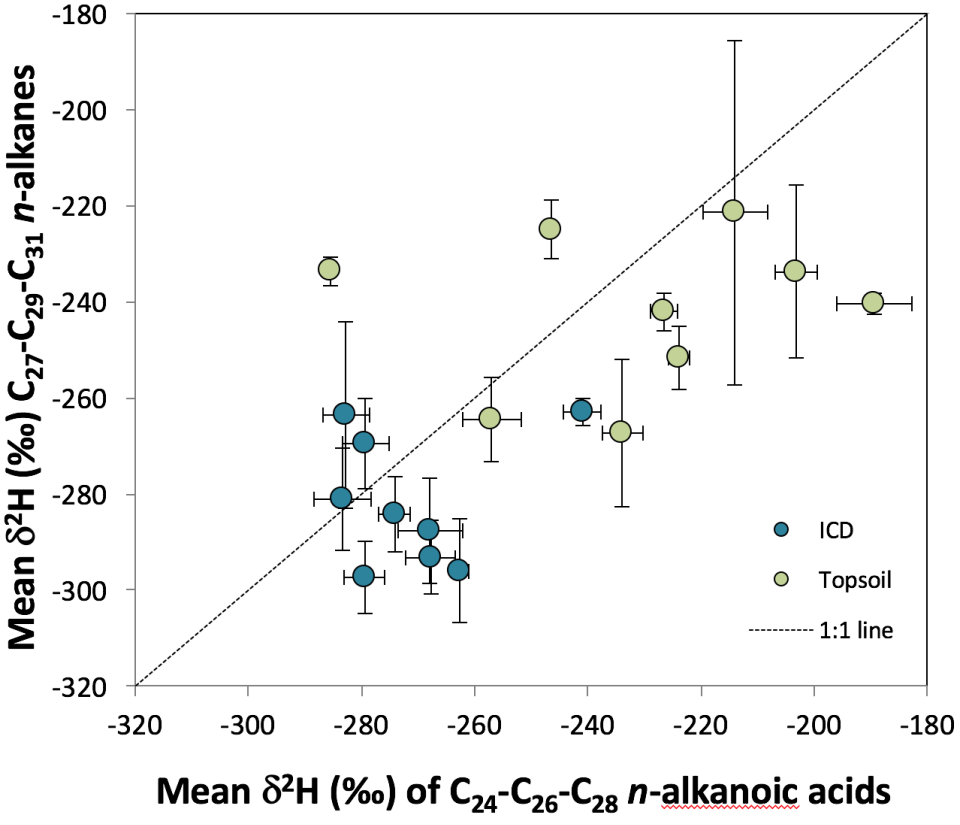

899
900

The Cryosphere Discuss., doi:10.5194/tc-2017-17, 2017
Manuscript under review for journal The Cryosphere
Discussion started: 21 February 2017

Figure 5

Comparison of δ^2H values of C_{28} *n*-alkanoic acid (left) and C_{29} *n*-alkane (right) in modern (Topsoil-PF; green circles) and ICD-PF for this study (blue circles) and available literature, with crosses from Zech et al. (2011; glacial and interglacial paleosoils from permafrost bluff exposure at Tumara River northeast Siberia), black triangles from Yang et al. (2011; C3 plants and trees from Canada and Alaska), light grey triangles from Wilkie et al. (2013; C3 plants from the El'gygytgyn lake basin, Siberia), white triangles from Pautler et al. (2014; modern and paleosoils from the Yukon territory, Canada) and dark grey triangles from Porter et al. (2016; muck deposits from the Yukon territory, Canada).

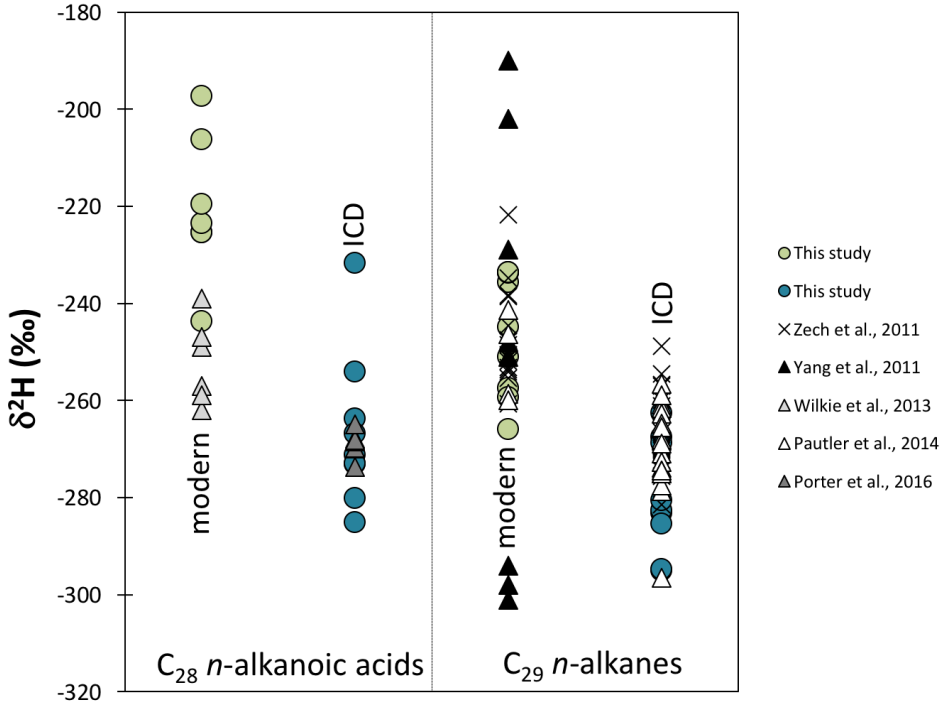

The Cryosphere Discuss., doi:10.5194/tc-2017-17, 2017
Manuscript under review for journal The Cryosphere
Discussion started: 21 February 2017

916 **Figure 6**
917 Contribution of OC from Topsoil-PF (green) and ICD-PF (blue) sources to surface
918 sediments along a shelf-slope transect in the Laptev Sea (see also Bröder et al., 2016b for
919 further transect information), calculated with a $\delta^{13}C$- $\Delta^{14}C$ (triangles) and leaf wax $\delta^{2}H$
920 mixing model (circles). Stations are plotted against log water depth (m; see also Table 6)
921 following the transect order from the coastal, nearshore, zone in the South (furthest left;
922 TB-46, 6 m depth) towards the continental rise in the North (furthest right; SW-01, 3146
923 m depth). Topsoil $\Delta^{14}C$ end-member values are corrected for cross-shelf transport time
924 (see section 4.2).
925

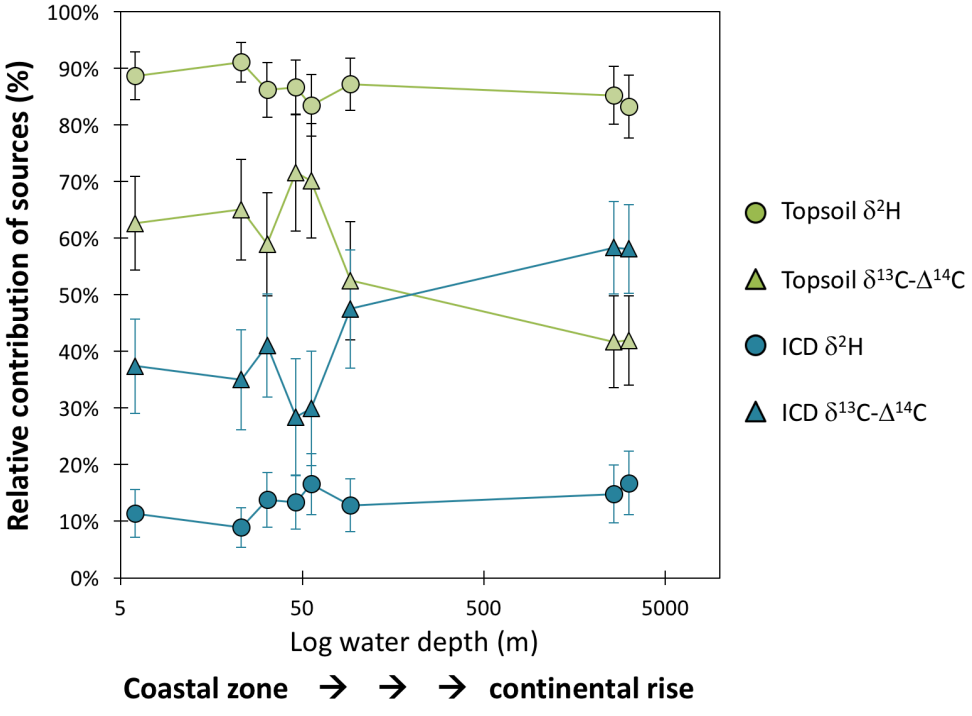

926

The Cryosphere Discuss., doi:10.5194/tc-2017-17, 2017
Manuscript under review for journal The Cryosphere
Discussion started: 21 February 2017

Table 1
Site characteristics and geochemical properties of eight topsoil and eight ice complex deposit samples. A table with more detailed sample descriptions can be found in Supplementary Table 1.

Sample ID	Current vegetation	Watershed	Description	Lat	Lon	TOC	$\delta^{13}C$	TN	C/N
				°N	°E	%	‰	%	
Topsoil (modern vegetation and O-horizon samples)									
KU EXP 1-1, 0-16 cm	Tundra	Lena	Surface O-horizon; 0-16 cm	72.34	126.29	11	-27.0	0.40	27.5
CH YED2, 0-4 cm	Tundra	Kolyma	Surface O-A horizon; 0-4 cm	69.46	161.79	17	-28.4	0.64	26.5
SP T3-3B,	Alas grassland	Lena	Alas soil (Mollisol), mix of O and A horizon	62.32	129.50	15	-27.9	1.40	10.7
SP T2-7,	Larch taiga	Lena	Taiga soil (turbel), mix of O and A horizon	62.25	129.62	13	-28.4	0.45	28.0
KY T2-3,	Tussock tundra	Indigirka	Tundra soil (turbel), O-horizon	70.83	147.48	29	-28.5	1.56	18.7
CH T2-1,	Tussock tundra	Kolyma	Tundra soil (turbel), mix of O, Ojj and Ajj horizons	69.44	161.77	21	-26.4	0.57	36.7
CH YED3, 0-10 cm	Larch taiga	Kolyma	Surface O-hor; 0-10 cm	68.77	161.41	39	-29.6	1.29	30.7
CH Medv grass[a]	Grass tundra	Kolyma	Vegetation	69.64	162.54	41	-25.2	1.47	27.8
CH Y4 grass[a]	Larch taiga	Kolyma	Vegetation	68.74	161.41	40	-28.5	2.42	16.6
Mean values						**25**	**-27.8**	**1.1**	**24.8**
Ice complex deposits									
KU EXP 1-3, 212-216 cm	Tundra	Lena	Very deep undisturbed yedoma ca. 10 m below surface	72.34	126.29	1.3	-27.5	0.08	15.7
CH YED1, 300-305 cm	Tussock tundra	Kolyma	Deep undisturbed yedoma ca. 3 m below surface	69.47	161.77	1.4	-26.3	0.14	10.2
CH YED2, 300-305 cm	Tussock tundra	Kolyma	Deep undisturbed yedoma ca. 3 m below surface	69.46	161.79	2.3	-25.8	0.27	8.6
CH YED3, 520-525 cm	Larch taiga	Kolyma	Deep undisturbed yedoma ca. 5 m below surface	68.77	161.41	1.4	-25.5	0.15	9.7
KY EXP1, 0-5 cm	Tussock tundra	Indigirka	Undisturbed yedoma ca. 2 m below surface	70.83	147.44	1.5	-25.5	0.18	8.5

The Cryosphere Discuss., doi:10.5194/tc-2017-17, 2017
Manuscript under review for journal The Cryosphere
Discussion started: 21 February 2017

The Cryosphere Discussions
Open Access
EGU

KY EXP2, 110-115 cm	Tussock tundra	Indigirka	Deep undisturbed yedoma ca. 4.5 m below surface	70.83	147.44	1.6	-25.6	0.19	8.6	
KY EXP3, 185-190 cm	Tussock tundra	Indigirka	Undisturbed yedoma ca. 2 m below surface	70.83	147.49	1.5	-25.2	0.17	8.5	
CH DY-3A	Larch taiga	Kolyma	Particulate matter from thaw streams	68.63	159.15	1.5[b]	-25.2[b]	-	-	
CH DY-4A	Larch taiga	Kolyma	Particulate matter from thaw streams	68.63	159.15	1.4[b]	-25.1[b]	-	-	
Mean values						**1.6**	**-25.7**	**0.2**	**10.0**	

a vegetation samples
b data from Vonk et al., 2013

The Cryosphere Discuss., doi:10.5194/tc-2017-17, 2017
Manuscript under review for journal The Cryosphere
Discussion started: 21 February 2017

Table 2
Long-chain *n*-alkane concentrations (in µg/gOC) of topsoil Holocene samples (modern vegetation/O-horizon) and Pleistocene ice complex samples.

	C21	C22	C23	C24	C25	C26	C27	C28	C29	C30	C31	C32	C33
	µg/g OC												
Topsoil (modern vegetation and O-horizon samples)													
KU EXP 1-1, 0-16 cm	44	88	96	45	41	10	45	4.4	27	2.5	36	1.5	7.2
CH YED2, 0-4 cm	24	15	21	12	40	10	160	10	150	6.5	150	3.5	17
SP T3-3B	2.5	2.4	5.9	2.6	13	4.7	42	16	74	4.7	85	2.7	24
SP T2-7	19	3.3	7.1	2.7	27	4.5	47	6.7	98	9.1	150	5.7	38
KY T2-3	35	8.4	26	9.9	38	13	91	18	180	14	230	8.1	43
CH T2-1	14	5.1	16	5.7	19	4.0	26	3.7	48	5.0	120	4.0	32
CH YED3, 0-10 cm	46	12	18	8.8	22	16	61	27	220	23	340	12	48
CH Medv grass	4.1	1.7	18	10	61	16	47	13	30	5.3	10	1.1	1.1
CH Y4 grass	4.7	2.6	18	15	45	21	50	16	31	6.8	9.8	1.5	2.6
Ice complex deposits													
KU EXP 1-3, 212-216 cm	57	79	100	49	82	23	170	16	137	8.5	140	4.4	25
CH YED1, 300-305 cm	55	89	100	70	70	27	75	20	130	12	120	5.3	28
CH YED2, 300-305 cm	40	64	74	31	54	15	79	22	110	10	160	4.8	32
CH YED3, 520-525 cm	60	93	98	47	55	20	84	22	140	12	150	6.0	39
KY EXP1, 0-5 cm	46	79	86	56	49	20	55	13	75	7.0	100	4.7	38
KY EXP2, 110-115 cm	41	73	87	68	62	29	65	20	98	11	120	4.9	27
KY EXP3, 185-200 cm	50	83	83	43	41	16	65	17	100	8.3	120	4.5	42
CH DY-3A	4.2	7.3	23	30	55	42	82	38	100	18	110	5.0	21
CH DY-4A	6.2	6.2	16	11	29	15	51	20	79	9.3	85	4.1	23

The Cryosphere Discuss., doi:10.5194/tc-2017-17, 2017
Manuscript under review for journal The Cryosphere
Discussion started: 21 February 2017

Table 3
Long-chain *n*-alkanoic acids concentrations (in µg/gOC) of topsoil Holocene samples (modern vegetation/O-horizon) and Pleistocene ice complex samples.

	C16	C18	C20	C21	C22	C23	C24	C25	C26	C27	C28	C29	C30
	µg/gOC												
Topsoil (modern vegetation and O-horizon samples)													
KU EXP 1-1, 0-16 cm	511	220	176	80.5	539	311	1100	4.95	684	90.5	350	32.8	58.1
CH YED2, 0-4 cm	1740	664	673	235	1380	496	1390	543	1740	409	1580	113	305
SP T3-3B	664	296	480	116	1020	504	1710	415	1550	250	1060	132	456
SP T2-7	1140	408	665	235	1400	431	1410	425	1250	242	651	143	455
KY T2-3	513	343	530	133	1140	359	1410	1.58	896	119	494	67.8	224
CH T2-1	1080	537	418	236	1420	790	2670	2.82	1570	127	657	46.6	174
CH YED3, 0-10 cm	1420	352	538	281	1850	722	2010	651	1790	642	1580	730	1971
CH Medv grass	3640	855	691	44.1	609	63.5	156	26.0	224	0.122	99.3	9.91	28.1
CH Y4 grass	4600	887	966	53.6	815	66.7	261	28.6	232	11.5	124	8.10	30.2
Ice complex deposits													
KU EXP 1-3, 212-216 cm	1750	1600	4560	1460	9460	2300	8930	2020	5830	1030	3660	293	635
CH YED1, 300-305 cm	10400	4030	5800	2410	17100	7270	18600	6610	16600	5860	14800	6810	18700
CH YED2, 300-305 cm	665	554	892	263	2070	1060	3070	646	2340	272	1310	133	532
CH YED3, 520-525 cm	1400	769	1030	252	2040	910	3120	644	2440	266	1160	124	432
KY EXP1, 0-5 cm	426	304	447	126	1220	511	1970	70.4	1390	133	712	60.7	233
KY EXP2, 110-115 cm	722	539	583	153	1370	606	2270	457	1970	181	1030	86.4	333
KY EXP3, 185-200 cm	446	313	543	158	1330	562	2350	401	1370	154	743	63.1	230
CH DY-3A	920	402	895	108	1070	294	1180	184	799	70.3	331	34.4	100
CH DY-4A	327	200	559	74	803	229	1010	2.17	718	64.9	334	28.7	104

Table 4
Sum of most abundant long-chain *n*-alkanoic acids and *n*-alkanes (concentrations in µg/gOC), and characteristic ratios of *n*-alkanoic acids and *n*-alkanes of topsoil Holocene (modern vegetation/O-horizon) and Pleistocene ice complex samples.

	***n*-alkanoic acids**				***n*-alkanes**			
	ΣHMW[a] (>C_{22}) *µg/gOC*	**ΣC_{22}-C_{28} (even)** *µg/gOC*	**CPI[b]**	**HMW acids/ HMW alkanes[a]**	**ΣHMW[a] (>C_{21})** *µg/gOC*	**ΣC_{25}-C_{31} (odd)** *µg/gOC*	**CPI[c]**	**C_{25}/ (C_{25}+C_{29})**
Topsoil (modern vegetation and O-horizon samples)								
KU EXP 1-1, 0-16 cm	3167	2670	5.8	7.1	447	148	2.7	0.60
CH YED2, 0-4 cm	7958	6090	3.8	13	612	494	11	0.21
SP T3-3B	7095	5340	4.1	25	280	214	7.2	0.15
SP T2-7	6397	4700	3.7	15	418	323	12	0.21
KY T2-3	4715	3940	6.8	6.6	717	543	9.1	0.17
CH T2-1	7454	6310	6.0	25	300	211	9.9	0.28
CH YED3, 0-10 cm	11950	7230	2.9	14	857	647	7.8	0.09
CH Medv grass	1216	1090	9.5	5.6	217	148	3.7	0.67
CH Y4 grass	1577	1430	11	7.1	223	135	2.5	0.59
Mean (median)	*5726 (6397)*	*4310 (4700)*	*5.9*	*13*	*452 (418)*	*318 (214)*	*7.3*	*0.33*
St.dev (IQR)	*3431 (4290)*	*2190 (4320)*	*2.7*	*7.6*	*230 (332)*	*195 (345)*	*3.6*	*0.22*
Ice complex deposits								
KU EXP 1-3, 212-216 cm	34854	27883	4.1	39	893	530	4.9	0.38
CH YED1, 300-305 cm	112356	67078	2.8	140	806	398	3.0	0.35
CH YED2, 300-305 cm	11430	8791	4.1	16	698	405	4.6	0.33
CH YED3, 520-525 cm	11145	8768	4.4	14	825	428	3.8	0.29
KY EXP1, 0-5 cm	6293	5285	6.5	10	630	280	2.9	0.40
KY EXP2, 110-115 cm	8293	6629	4.9	12	708	347	2.7	0.39
KY EXP3, 185-200 cm	7196	5787	4.7	11	671	323	3.5	0.29
CH DY-3A	4063	3380	5.5	7.6	533	344	2.7	0.35
CH DY-4A	3295	2867	8.3	9.3	355	244	4.3	0.27
Mean	*22103 (8290)*	*15160 (6630)*	*5.0*	*29*	*680 (698)*	*367 (347)*	*3.6*	*0.34*
St.dev	*35150(5140)*	*20880 (3510)*	*1.6*	*43*	*163 (176)*	*85 (81)*	*0.8*	*0.05*

a HMW; high-molecular weight
b CPI; carbon preference index for chain lengths C_{22}-C_{28}, for calculation see caption of Fig. 2.
c CPI; carbon preference index for chain lengths C_{23}-C_{31}, for calculation see caption of Fig. 2.

The Cryosphere Discuss., doi:10.5194/tc-2017-17, 2017
Manuscript under review for journal The Cryosphere
Discussion started: 21 February 2017

Table 5
δ^2H signatures (in ‰) of *n*-alkanoic acids and *n*-alkanes of topsoil Holocene (modern vegetation/O-horizon) and Pleistocene ice complex samples.

	***n*-alkanoic acids**							***n*-alkanes**			
	C16	**C18**	**C20**	**C22**	**C24**	**C26**	**C28**	**C25**	**C27**	**C29**	**C31**
Topsoil (modern vegetation and O-horizon samples)											
KU EXP 1-1, 0-16 cm	-162	-180		-119	-178	-203	-197	-168	-240	-236	-244
CH YED2, 0-4 cm	-188	-192		-211	-222	-232	-225	-196	-237	-251	-239
SP T3-3B				-126	-203	-218	-225		-125	-234	-259
SP T2-7	-171	-213		-180	-196	-210	-206		-182	-245	-243
KY T2-3		-235	-185	-253	-257	-264	-244	-164	-240	-266	-273
CH T2-1	-189	-222		-214	-235	-236	-224	-203	-221	-258	-282
CH YED3, 0-10 cm	-184		-190	-218	-227	-225	-220	-199	-234	-259	-250
CH Medv grass	-258	-246	-253	-256	-285	-286		-253	-236	-234	-224
CH Y4 grass	-237	-244	-251	-248	-245	-248		-227	-223	-234	-209
Mean	*-199*	*-219*	*-220*	*-203*	*-228*	*-236*	*-220*	*-201*	*-215*	*-246*	*-247*
St.dev	35	25	37	52	33	27	15	*32*	*39*	*13*	*23*
Ice complex deposits											
KU EXP 1-3, 212-216 cm	-194	-227	-243	-252	-245	-241	-232	-237	-257	-268	-265
CH YED1, 300-305 cm			-231	-264	-271	-280	-271	-217	-266	-283	-297
CH YED2, 300-305 cm				-249	-262	-278	-264	-254	-279	-283	-307
CH YED3, 520-525 cm			-209	-252	-266	-277	-254	-243	-261	-285	-305
KY EXP1, 0-5 cm			-169	-260	-275	-288	-273	-189	-245	-269	-283
KY EXP2, 110-115 cm	-211	-216	-252	-266	-274	-294	-285	-192	-254	-281	-296
KY EXP3, 185-200 cm			-191	-263	-277	-287	-273	-210	-279	-295	-309
CH DY-3A	-244	-256	-277	-277	-277	-293	-280	-195	-221	-263	-298
CH DY-4A	-228	-229	-261	-265	-262	-262	-267	-251	-270	-295	-313
Mean	*-219*	*-232*	*-229*	*-261*	*-268*	*-278*	*-267*	*-221*	*-259*	*-280*	*-297*
St.dev	21	17	37	8.6	10	17	16	*26*	*18*	*12*	*15*

The Cryosphere Discuss., doi:10.5194/tc-2017-17, 2017
Manuscript under review for journal The Cryosphere
Discussion started: 21 February 2017

Table 6
Location, sampling depth and isotopic values of samples along a surface sediment transect in the Laptev Sea (data from Bröder et al., 2016b), with percentage topsoil (TS) and ice complex deposit (ICD) OC contributions to the samples based on source-apportionment calculations with δ^2H leaf wax end-members versus $\delta^{13}C$-$\Delta^{14}C$ end-members (end-member values are described in the text).

				Sample values						**Source contributions**			
ID[a]	**Lat**	**Long**	**Depth**	**C_{27}**	**C_{29}**	**C_{31}**	**$C_{27\text{-}29\text{-}31}$**[b]	**$\delta^{13}C$**	**$\Delta^{14}C$**	**TS**	**ICD**	**TS**[c]	**ICD**[c]
	N	°E	m	‰	‰	‰	‰	‰	‰	using δ^2H		using $\delta^{13}C$-$\Delta^{14}C$	
TB-46	72.700	130.180	6	-236.2	-237.4	-230.4	-235.0	-26.5	-436	89%	11%	63% (63%)	37% (37%)
YS-9	73.366	129.997	23	-233.7	-231.0	-227.8	-231.1	-26.1	-415	91%	8.9%	63% (65%)	37% (35%)
YS-6	74.724	130.016	32	-234.2	-241.0	-235.4	-236.8	-25.6	-465	86%	14%	51% (59%)	49% (41%)
SW-24	75.599	129.558	46	-229.3	-236.5	-243.5	-236.4	-24.8	-284	87%	13%	70% (72%)	30% (28%)
SW-23	76.171	129.333	56	-219.9	-243.3	-243.3	-236.0	-25.0	-333	83%	17%	65% (70%)	35% (30%)
SW-06	77.142	127.378	92	-219.5	-237.0	-241.4	-233.2	-23.2	-364	87%	13%	39% (53%)	61% (47%)
SW-03	78.238	126.150	2601	-221.1	-238.0	-247.7	-235.9	-22.6	-426	85%	15%	23% (42%)	77% (58%)
SW-01	78.942	125.243	3146	-223.8	-241.8	-246.0	-238.0	-22.3	-418	83%	17%	21% (42%)	79% (58%)

a Location, depth and bulk carbon isotope data from Bröder et al. (2016b)
b weighted average based on individual concentrations
c numbers in brackets are source contributions using the $\delta^{13}C$-$\Delta^{14}C$ approach but with additional corrections for cross-shelf lateral transport time of topsoil OC (similar as in Bröder et al., 2016a); we applied linear aging along the transect based on the distance from the coast, with a maximum aging of 5000 years for station SW-01.